A focus on epitranscriptomics and aging: The effect of $m^6A_{(m)}$ modulation on C/EBPβ isoform expression

Pau Garcia Baucells

M.Sc. Biomedical Sciences | **Biology of Aging** | **Rijksuniversiteit Groningen**

Research Internship I

2021 – 2022

Supervised by Christine Müller

European Research Institute for the Biology of Aging (ERIBA)

Calkhoven group – Gene regulation in ageing and age-related diseases

Universitair Medisch Centrum Groningen (UMCG)

rijksuniversiteit groningen

umcg

TABLE OF CONTENTS

Abstract

The transcription factor C/EBPβ gives rise to three different isoforms with antagonizing effects. The ratio of such isoforms has been proven to mediate biological processes like aging, cancer, or metabolism. Because of this, understanding the molecular mechanisms that govern or control C/EBPβ's isoform expression is relevant and necessary. One important form of regulation is the epitranscriptome, which consists of a wide range of chemical modifications in RNA that are able to determine key features of RNA biology such as splicing, stability or decay. In the present study, we aimed at elucidating the effect of $m^6A_{(m)}$ transcript modulation in the isoform expression of C/EBPβ; adenosine decorations that confer a methylome signature controlled by methyltransferases (writers) and demethylases (erasers). To test this, we overexpressed and knocked-down the existing writers and erasers in three different cell lines and analyzed C/EBPβ's isoform expression. We report that total C/EBPβ protein content is sensitive upon modulation of several players, and notably, WTAP, FTO and ALKBH5 interfere with C/EBPβ's isoform expression. In the present work we discuss whether our observations illustrate direct effects of the $m^6A_{(m)}$ signature of C/EBPβ's transcript and we expand the understanding of its epitranscriptome and consequent mRNA regulation: pivotal aspects for developing healthspan-aimed therapeutics.

Introduction

C/EBPβ*: aging, cancer and metabolism*

CCAAT/enhancer-binding proteins (C/EBPs) make up a family of homologous transcription factors termed C/EBPα, C/EBPβ, C/EBPγ, C/EBPδ, C/EBPε and C/EBPζ (Cao et al., 1991; Lekstrom-Himes & Xanthopoulos, 1998). C/EBPs share a modular structure consisting of a transactivating domain, a DNA-binding domain, a regulatory domain and a highly conserved basic-leucine zipper (bZIP) domain that allows homo or heterodimerization, upon which C/EBPs are able to bind to negatively-charged (i.e., acidic) DNA and thus modulate gene expression (Wang et al., 2019). The transactivating domain, located in the N-terminus, mediates interaction with other proteins that can ultimately promote activation or repression of target gene transcription (Tsukada et al., 2011). C/EBPs have been identified to participate in a plethora of biological processes, such as inflammation, adipogenesis, energy metabolism, liver metabolism, hematopoiesis, tumorigenesis or cellular proliferation and differentiation (Ramji & Foka, 2002; Tsukada et al., 2011; Wang et al., 2019).

The family member C/EBPβ, on which the present study is focused, is encoded by a single exon gene that gives rise to different protein isoforms through usage of differential translation start sites (Calkhoven et al., 2000; Nerlov, 2010). As a transcription factor, C/EBPβ is highly expressed in the liver, adipose tissue, intestine or lungs, among others (Ramji & Foka, 2002); and it has been described to target a wide range of genes (assessed in: ENCODE Transcription Factor Targets dataset). Despite C/EBPβ's intronless nature, its mRNA is translated into three different protein isoforms and a single oligopeptide: Liver-enriched Activating Proteins (LAP1 and LAP2), Liver-enriched Inhibitory Protein (LIP) and a short peptide (11 amino acids in human and 9 in rodents) arising from an upstream Open Reading Frame (uORF) (Descombes & Schibler, 1991; Calkhoven et al., 2000; Tsukada et al., 2011). These isoforms are translated from four consecutive AUG codons located in the same transcript (**Fig. 1**) (Wethmar et al., 2010). LAP1 and LAP2 isoforms arise from standard translation, yet LAP1 is often skipped by scanning ribosomes given that its start codon lacks a Kozak consensus sequence (Kozak, 1987; Zidek et al., 2015). On the 5'UTR of the transcript, a *cis*–regulatory out of frame uORF controls the translation of the short peptide, which allows the ribosome's small subunit (40S) to remain attached to the transcript after termination at the uORF STOP codon and to scan further along the mRNA until a fourth in–frame start codon (AUG-LIP) is encountered. Reloading of the ribosomal's large subunit (60S) allows the complete 80S ribosome to start translation of the LIP isoform; and, indeed, *in vivo* deletion of the uORF (C/EBPβ$^{\Delta uORF}$ mice) results in reduced CEBPβ–LIP expression (Calkhoven et al., 2000; Wethmar et al., 2010; Zidek et al., 2015). LAP1, LAP2 and LIP share the C-terminus, which contains the DNA binding and dimerization bZIP domains. Nonetheless, LIP lacks the transactivation domain, and therefore is considered to be a competitive inhibitor of LAP1/2 isoforms as it is unable to recruit other coregulator proteins, yet alternative functions have also been described (Zidek et al., 2015; Bégay et al., 2018; Wang et al., 2019). All three isoforms are functionally different, which is the reason why the isoform ratio between LAP1/2 and LIP (hereby termed the LIP:LAP ratio) is key in determining the physiological effects of C/EBPβ (Niehrs & Calkhoven, 2019; Sterken et al., 2022; Zuidhof et al., 2022-A).

Complementary to C/EBPβ–LIP's regulation at the mRNA level, its translation efficiency is also regulated by the mTORC1 signaling pathway (Calkhoven et al., 2000; Jundt et al., 2005; Wethmar et al., 2010; Zidek et al., 2015), a key regulator of health- and lifespan (Johnson et al., 2013). Initial evidence hinted towards an eIF-2α

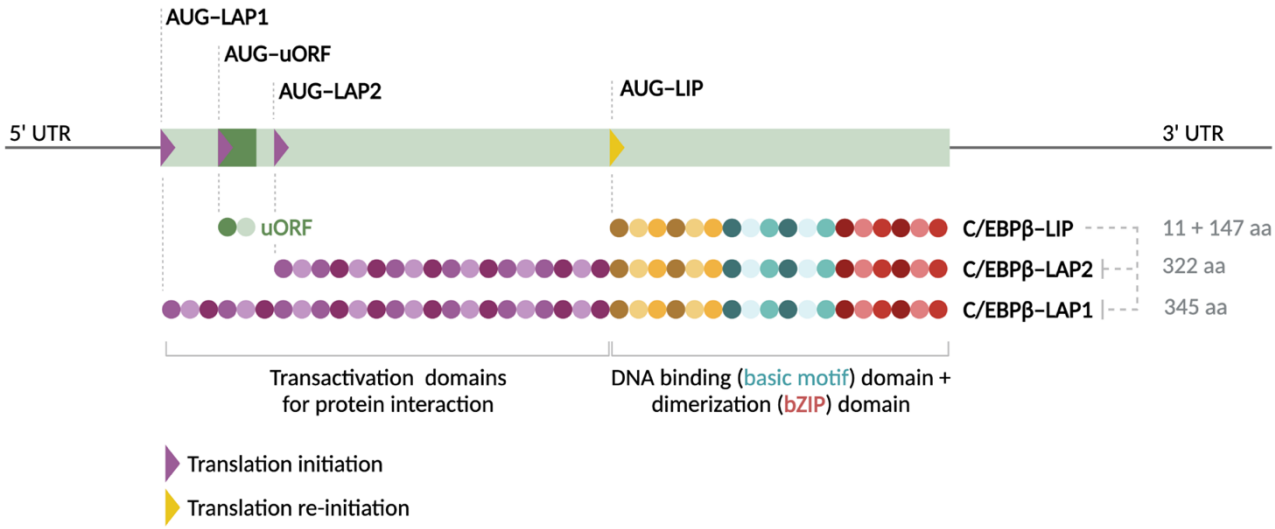

Figure 1. Illustrative representation of *CEBPB*'s mRNA structure aligned to the three C/EBPβ protein isoforms. Both C/EBPβ–LAP1 and LAP2 are translated through classical ribosomal initiation from their respective AUG codons (they differ by only 23 amino acids), yet LIP's translation requires a translation re-initiation event promoted by the uORF translation. After the uORF termination, the small ribosomal subunit stays attached to the mRNA due to the short size of the resulting peptide, and resumes re-scanning skipping AUG–LAP2 provided it is only 4 nucleotides downstream successively after the uORF's stop codon. Ribosomal reloading with new initiator tRNA will have taken place before the (in-frame) AUG–LIP is reached, reason why the resulting protein sequence is identical to the C-terminus fragment of LAP1/2. Thus, LIP differs from LAP1/2 in the N-terminus where the transactivating domains are included, which is the reason why it is thought to antagonize LAP1/2's function. *aa,* amino acid; *bZIP,* basic Leucine Zipper Domain; *uORF,* upstream Open Reading Frame; *UTR,* Untranslated Region.

and eIF-4E–mediated LIP regulation, the latter being downstream of mTORC1 (Calkhoven et al., 2000). Later on, Zidek and colleagues showed that rapamycin-mediated mTORC1's inhibition reduced LIP:LAP ratios *in vivo*. More importantly, LIP was also seen to be reduced in mice following caloric restriction (CR); which aside from their diminished C/EBPβ–LIP signature they also resemble C/EBP$\beta^{\Delta uORF}$ mice phenotypically (Zidek et al., 2015). These results first indicated that healthy-aging therapies like CR could be partly explained by the effect of mTORC1's downstream gene regulators like C/EBPβ. Indeed, further evidence not only demonstrated that LIP:LAP increases with age in mice but also that age-related pathologies are delayed in C/EBP$\beta^{\Delta uORF}$ mice; with females exhibiting ~21% extended median survival, delayed cancer incidence and improved tumor survival (Müller et al., 2018). Conversely, mice overexpressing LIP (thus having a high LIP:LAP ratio) are cancer prone and display a median survival of around 7 months less than the controls (Bégay et al., 2015). Furthermore, replacement of *Cebpa* by a second copy of *Cebpb* increased mice lifespan by ~5 months compared to heterozygous controls (Chiu et al., 2004), and C/EBP KO mouse models resemble progeroid models in multiple aspects such as weight reduction, decreased GH/IGF axis signaling or lipodystrophy (Schäfer et al., 2018; Niehrs & Calkhoven, 2019). All these findings suggest that a high C/EBPβ–LIP:LAP ratio promotes cancer and shortened lifespan, a low LIP:LAP is a protective factor for such phenotype, and that C/EBPβ's isoform expression changes during aging. With this, C/EBPβ might prove to have causal or contributive roles in the acquisition of age-related phenotypes and aging itself.

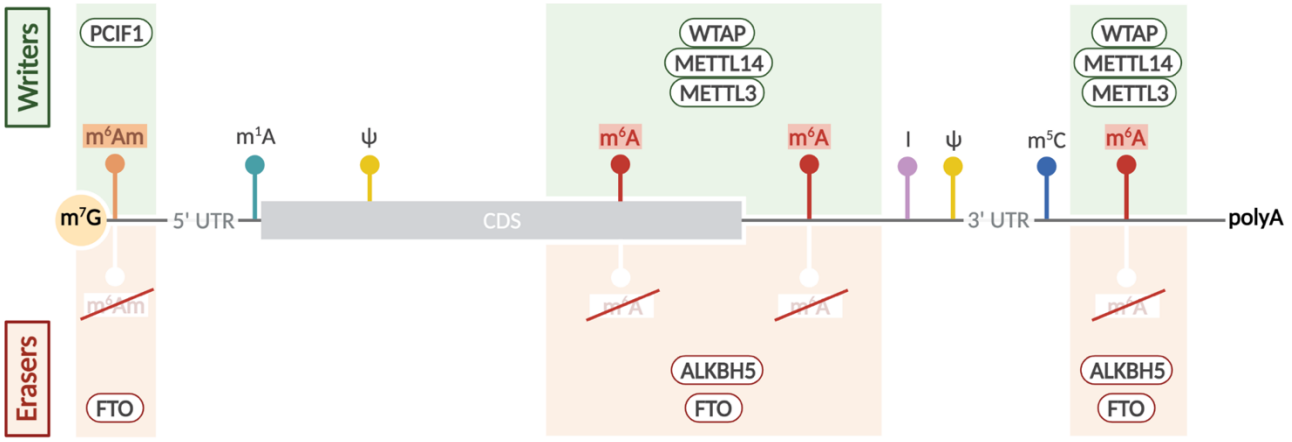

Figure 2. Schematic depiction of selected epitranscriptomic modifications of mRNA with focus on $m^6A_{(m)}$–modulating proteins. The epitranscriptome confers a malleable layer for added RNA regulation. m^6A-decoration is conferred through the catalytically active METTL3, which associates to METTL14 and WTAP, though several other proteins have been linked to the complex. ALKBH5 and FTO are the corresponding m^6A demethylases, with FTO also having the cap-associated m^6A_m as substrate. This highly dynamic interplay between the writer complex and the erasers provides mRNA transcripts with regulatory potential. *CDS*, coding sequence; *m^7G*, N^7-methylguanosine; *m^6A*, N^6-methyladenosine; *m^1A*, N^1-methyladenosine, *ψ*, pseudo-uridine; *I*, inosine; *m^5C*, 5-methylcytidine; *m^6A_m*, N^6-2'-O-dymethyladenosine;

$m^6A_{(m)}$ mRNA modulation

Having seen the importance of translational control for the isoform expression of C/EBPβ, and thereby its resulting function, the question of whether post-transcriptional modifications of the *CEBPB* mRNA modulate the LIP:LAP ratio remains. One such form of regulatory potential lies in post-transcriptional RNA modifications, hereby termed collectively as the epitranscriptome. Since the discovery of the first RNA modification in 1951 (Cohn & Volkin, 1951), as many as 170 different chemical alterations have been identified in all kinds of RNA species up until today (Koh et al., 2019). The epitranscriptome can affect RNA splicing, stability and turnover, translation efficiency or localization; ultimately affecting gene expression (Dominissini et al., 2012; Schöller et al., 2018). Some of these modifications include N^6-methyladenosine (m^6A), N^1-methyladenosine (m^1A), pseudo-uridine (ψ), inosine (I), 5-methylcytidine (m^5C) or N^6-2'-O-dymethyladenosine (m^6A_m) (**Fig. 2**) (Li et al., 2017; Wiener & Schwartz, 2021). New high-throughput sequencing methods (Meyer et al., 2012) allowed the identification of m^6A as the most prevalent modification in mRNA, with effects ranging from regulation of gene expression to human pathology (Maity & Das, 2016; Shi et al., 2019). Deposition of the m^6A mark is sequence specific in 77% of the cases (RRACH; R = G/A, H = A/C/T), and is asymmetrically and preferentially found at the 3' UTR, around stop codons and the coding sequence (CDS) (Linder et al., 2015; Ben-Haim et al., 2021). Indeed, the *CEBPB* transcript contains 19 RRACH sequences prevalently located at the CDS and 3' UTR, yet only a fraction of all possible consensus sites in mRNA species are found to be methylated (Zaccara et al., 2019).

Regulation of the m^6A mRNA decoration is dependent on two main groups of players: the writers (methyltransferases) and the erasers (demethylases) (**Fig. 2**). The multi-subunit methyltransferase complex consists of the catalytically active methyltransferase-like 3 (METTL3), the RNA-binding methyltransferase-like 14 (METTL14) and the anchoring adaptor Wilms' Tumor 1-Associating Protein (WTAP), which altogether form the resulting METTL3/14-WTAP complex that is able to methylate adenosines in the newly synthesized transcript (Schöller et al., 2018; Zaccara et al., 2019). Nonetheless, several other components like VIRMA,

RBM15/15B, ZC3H13 or HAKAI provide both regulation and specificity to m^6A modifications (Zaccara et al., 2019; Shi et al., 2019). On the other hand, erasers (namely FTO and ALKBH5) are able to oxidatively demethylate m^6A into A. FTO (fat mass and obesity associated) was the first gene with common polymorphisms associated with susceptibility to obesity through GWAS studies (Frayling et al., 2007; Loos et al., 2014). Despite unclear consensus over its main biological substrate, FTO is accepted to demethylate both m^6A and m^6A_m residues (Mauer et al., 2017). m^6A_m takes place in the first transcribed adenosine consecutive to the 5' cap, a reaction catalyzed by PCIF1/CAPAM through methylation of A_m (Akichika et al., 2019; Boulias et al., 2019; Ben-Haim et al., 2021). Given that FTO has been shown to have as much as 100 times higher affinity to demethylate m^6A_m in biochemical assays than m^6A, FTO overexpression *in vivo* consistently demethylates decorated adenosines throughout the whole transcript (Mauer et al., 2017; Zhou et al., 2018; Zaccara et al., 2019). Identification of entacapone as an FTO inhibitor demonstrated increased m^6A marks in the CDS of mRNA (Peng et al., 2019). On the other hand, the other eraser AlkB homolog 5 (ALKBH5) only has activity towards m^6A, and its expression among tissues differs with that of FTO's (Shi et al., 2019). All in all, and despite the redundant demethylase activities from FTO and ALKBH5, the $m^6A_{(m)}$ epitranscriptome seems to be a tightly controlled layer of gene regulation.

The effect of m^6A decoration relies on reader RNA-binding proteins that are able to bind to such sites and carry out diverse functions (Kretschmer et al., 2018). These functions include promoting alternative splicing, transcript stability or degradation, RNA secondary structure alteration, subcellular localization, translation and others (Zhu et al., 2020). Some of the identified readers include the group of YT521-B homology (YTH) domain-containing proteins and insulin-like growth factor 2 binding proteins (IGF2BP) (Huang et al., 2018).

Since the publication of the Hallmarks of Aging, many critics have pointed out that other features of the aging process remain left out (Lopez-Otín et al., 2013; Gems & de Magalhães, 2021). One such feature corresponds to the epitranscriptomic changes that the transcriptome experiences through lifetime. In this context, the $m^6A_{(m)}$ methylome has been described to decrease in peripheral blood mononuclear cells with increasing age (Min et al., 2018), and both METTL3 and m^6A were reduced in prematurely senescent stem cells (Wu et al., 2020). These findings point towards a highly overlooked feature of aging that requires new insights (McMahon et al., 2021). Indeed, the *CEBPB* transcript has recently been described to only harbor a 5' UTR m^6A modification (Sun et al., 2021), which was not found in another study (Boulias et al., 2021). Nevertheless, prior evidence detected four m^6A peaks at the CDS and the 3' UTR (Linder et al., 2015; Hu et al., 2022), and non-5' UTR m^6A peaks at the CDS and 3' UTR were found in both lean and HFD-fed mice (Ben-Haim et al., 2021). In this line, Zhou and colleagues demonstrated that m^6A elimination in the 5' UTR of the ATF4 gene promotes a uORF-mediated translation reinitiation event, thereby promoting ATF4 translation (Zhou et al., 2018). All in all, whether C/EBPβ's isoform expression regulation is also dependent on $m^6A_{(m)}$ mRNA decoration, and whether such regulation is responsible for its age-related changes is unknown.

Here, we set out to unravel the contribution of the main $m^6A_{(m)}$ epitranscriptomic players to the isoform expression of C/EBPβ, in aims of understanding the biology of C/EBPβ. Considering C/EBPβ's implication in cancer, metabolism and aging through the changes in its isoform expression; by elucidating the mechanisms that govern this process we will be able to come up with new mechanisms to promote a low and healthy C/EBPβ–LIP:LAP ratio. In this line, finding relevant targets or processes that could be used for intervention would prove to be crucial for a wide range of pathologies. By using cell culture and molecular biology techniques we demonstrated that m^6A–decorating enzymes tend to increase total C/EBPβ content and that WTAP, FTO and ALKBH5 participate in the modulation of C/EBPβ's isoform expression *in vitro*.

Materials and Methods

Experimental cell culture, freezing and harvesting

Adherent cell lines were cultured at 37ºC and 5% CO_2 (Heracell™ 240i CO_2 Incubator) in either Greiner® Bio-one or TPP® 6 cm, 10 cm or 15 cm cell culture dishes and periodically split in aims of avoiding cellular crowding through PBS washing and dissociating agent Gibco™ Trypsin-EDTA (0.05%); discarding excess (serum-inactivated) trypsin through low-speed centrifugation (1.200 rpm, 5 min). HEK293T, BT20 and MDA-MB-231 cell lines were cultured in Gibco™ DMEM, supplemented with GlutaMAX™, sodium pyruvate and high glucose; the MCF-7 cell line was cultured in Gibco™ RPMI 1640 Medium, supplemented with GlutaMAX™ and sodium pyruvate. All mediums were supplemented with 10% TICO Europe EU–Approved Fetal Bovine Serum (FBS) and Gibco™ Penicillin-Streptomycin; and HEPES when indicated.

Cells were routinely examined in Leica®'s Inverted Laboratory Microscope DMIL LED and occasionally tested for mycoplasma infection. Cell counting was performed in either Bio-rad®'s TC20™ Automated Cell Counter or Neubauer chambers.

Cell lines were frozen in 10% EDTA in FBS and stored at -80ºC. For harvesting, cells were twicely washed in cold PBS in non-sterile conditions, scraped and pelleted at 12.000 rpm for 30 seconds at 4ºC. Next, pellets were snap–frozen in liquid nitrogen (-196ºC) and stored at -80ºC for downstream applications.

Western Blotting

Cellular extracts were lysed with RIPA buffer (radioimmunoprecipitation assay buffer) and successively mechanically disrupted through sonication (8 cycles of 60 seconds each) for successful lysis and cell membrane disruption. Bradford Assays were conducted in aims of loading equal amounts of protein for each cell line and experimental setting (ranging from 50 to 70 µg per sample). Either PerfectBlue™ 12% acrylamide M-sized Vertical Double Gel Systems or Bio-Rad® 4–20% Mini-PROTEAN® TGX™ Precast Protein Gels were loaded with the corresponding samples. Bio-Rad® Immun-Blot® PVDF or Nitrocellulose membranes (pore size: 0.2 µm) were used, and activated with methanol for the case of PVDF. Gel-to-membrane transfer was performed with Bio-Rad®'s Trans-Blot Turbo Transfer System. Membranes were afterwards blocked in 5% skimmed milk in 1X Tris-Buffered Saline 0.5% Tween® 20 Detergent (TBST), equilibrated and incubated with commercially-obtained primary antibodies (**Suppl. Table 1**). After overnight incubation with the selected primary antibody, four consecutive washes with TBST were done. Next, Amersham™ ECL™ anti-rabbit or anti-mouse (depending on primary antibody) IgG secondary antibody linked to horseradish peroxidase incubation (1:5000) was carried out for 1h at room temperature. Four extra TBST washes were done afterwards prior to membrane developing. Amersham ImageQuant™ 800 Western Blot Imaging was utilized to detect chemiluminescence signal from ECL–treated membranes (Western Lightning® Plus-ECL), in exposure intervals ranging from 1 to 25 minutes depending on the primary antibody used. Membrane stripping was done with ThermoFisher Scientific® Restore™ Western Blot Stripping Buffer.

ImageQuant™ was used for Western Blot quantification. LIP:LAP ratios were calculated by dividing the LIP fraction over the LAP1/2 fraction(s) as a mean of relativizing the amount of C/EBPβ–LIP in each sample. Statistical analysis was performed as indicated on each figure.

RT-qPCR

RNA isolation was carried out with Qiagen® RNeasy Plus Mini Kit, directly from frozen cell pellets obtained from harvested single 10 cm cell culture plates. Genomic DNA (gDNA) was effectively removed through gDNA Eliminator columns included in the kit and 1% β-mercaptoethanol was added to the lysis buffer for RNase

inactivation. RNase-free handling conditions were cautiously adopted for optimal RNA obtention at all times. The obtained RNA was kept at -80ºC for subsequent complementary DNA (cDNA) synthesis or mRNA isolation.

Synthesis of cDNA was performed with Roche®'s Transcriptor First Strand cDNA Synthesis Kit, by using an input concentration of 1000 ng of RNA and according to the manufacturer's denaturation, annealing and extension temperature indications.

RT-qPCR was run with 1:25 diluted cDNA samples and the corresponding primers (**Suppl. Table 2**). Promega®'s GoTaq® RT-qPCR kit was used, containing 2X SYBR® Green I, according to the manufacturer's denaturation, annealing and extension temperature indications. Dilution curves of mixed samples were done in aims of obtaining linear regression values for each primer pair, altogether with normalization to both actin and the specified controls for data representation.

Lentiviral infection

Lentivirus infection of target cells was performed by using virus-containing medium filtered through 0.45µm pore-sized membrane filters; obtained from HEK293T producer cells. Transfection of producer cells was executed by delivery of 10 µg of the corresponding transfer vector (in either *pLKO.1–puro* or *pLVX-IRES-neo*^{R} backbones), 6.5 µg of packaging plasmid pMDL-REE, 3.5µg of envelope plasmid pCMV-VSVg and 2.5µg of Rev-encoding plasmid pRSV-Rev in the presence of $CaCl_2$ and 2x HEPES Buffered Saline (HeBS) buffer. Antibiotic selection was conducted on day 2 after infection of target cells with corresponding antibiotic depending on the transfer vector used: Gibco™ Geneticin™ Selective Antibiotic (G418 Sulfate) was used to select *pLVX-IRES-neo*^{R}–infected cells at concentrations 1.200, 1.000 and 800 µg/mL (BT20, MDA-MB-231 and MCF-7 respectively); Sigma-Aldrich® puromycin dihydrochloride was used to select *pLKO.1*–infected cells at concentrations 1, 0.5 and 0.5 µg/mL (BT20, MDA-MB-231 and MCF-7 respectively).

Gene cloning

FTO (*FTO* wt) and the catalytically inactive *FTO* (*FTO* mut; R316.322Q) were cloned into the HIV1-based *pLVX-IRES-neo*^{R} vector from *FTO* wt/*FTO* mut–*pcDNA3.1+* through the digestion of the latter with NheI HF and XbaI restriction enzymes. The *pLVX-IRES-neo*^{R} vector was digested solely with XbaI for consequent ligation.

METTL14 was cloned into the *pLVX-IRES-neo*^{R} vector from *METLL14–pcDNA3.1* through digestion of both backbones with EcoRI HF + XbaI.

METTL3 was PCR-amplified in two fragments (**Suppl. Table 3**) from an MCF-7 cell line cDNA template and digested with HindIII + EcoRI HF and EcoRI HF + Xba I respectively, and cloned into two equally-digested *pBluescript II KS+* vectors. Both fragments were ligated with EcoRI HF and XbaI digested constructs to form the complete *METTL3* sequence in *pBluescript II KS+*. Consequently, it was cloned into pcDNA3.1+ (HindIII + XbaI) and into XbaI-digested *pLVX-IRES-neo*^{R} (from *pcDNA3.1+*, NheI HF + XbaI).

WTAP was PCR-amplified in two fragments (**Suppl. Table 3**) from an MCF-7 cell line cDNA template and digested with AatII + EcoRI HF and XbaI + AatII respectively, and cloned into two equally digested *pGEM®-7Zf(+)* vectors. Both fragments were ligated in a two insert, one vector fashion (in *pcDNA3.1+*, EcoRI HF + XbaI); and the complete *WTAP* in *pcDNA3.1+* was ultimately cloned into XbaI-digested *pLVX-IRES-neo*^{R} (NheI HF + XbaI).

Finally, *ALKBH5* was PCR-amplified as a single fragment (**Suppl. Table 3**) from an MCF-7 cDNA template and digested with EcoRI HF + XbaI, and cloned into equally-digested pBluescript II KS+. The latter was digested with XhoI + XbaI in order to be cloned into *pLVX-IRES-neo*^{R} (same restriction enzyme treatment); and digested with EcoRI HF + XbaI for *pcDNA3.1+* cloning.

All ligations of both digested vectors and inserts were carried out through 1:20 (Roche®) T4 DNA ligase with corresponding ligase buffer. Transformation of ligated constructs was performed in TOP10F competent *Escherichia coli*, selection made in 50 or 100 µg/mL ampicillin agar plates depending on construct size (lower selection pressure for bigger vectors like *pLVX-IRES-neo*^{R}).

Entacapone treatment

BT20, MDA-MB-231 and MCF-7 cell lines were treated with either 10 µM or 50 µM entacapone for 24, 48 and 72 hours prior to harvesting. DMSO-treated cells served as the control. Cell seeding was performed at decreasing concentrations so cellular confluency would not influence the results during the different lengths of the experiment: BT20: $1{\cdot}10^6$ (24h), $0{,}7{\cdot}10^6$ (48h), $0{,}5{\cdot}10^6$; MDA-MB-231: $1{,}5{\cdot}10^6$ (24h), $1{\cdot}10^6$ (48h), $0{,}7{\cdot}10^6$ (72h); MCF-7: $0{,}9{\cdot}10^6$ (24h), $0{,}6{\cdot}10^6$ (48h), $0{,}5{\cdot}10^6$ (72h) cells per 10 cm dish.

mRNA isolation and m^{6}A dot blotting

Total RNA was isolated as described before, and mRNA extracted with Thermofisher®'s Dynabeads™ Oligo(dT)25. A final amount of 26,5 ng/µL was diluted across all samples and denatured at 95ºC. 2 µL were used to spot dots in Amersham™'s Hybond™-N$^+$ positively charged nylon membrane and afterwards crosslinked with Stratlinker® UV crosslinker (twice at 120.000 µJ/cm^2). A successive washing step with TBST was carried out, and for loading control a wash with 0,05% methylene blue in 0,5M acetic acid was performed. Five distilled water washes (2 minutes each) were done in aims of improving the signal-to-background noise ratio and finally blocked with 5% BSA in TBST for an hour and later incubated overnight (4ºC) with the N^6-methyladenosine primary antibody (**Suppl. Table 1**). After overnight incubation, TBST washing and secondary antibody (1:5000 Amersham™ ECL™ anti-rabbit IgG secondary antibody linked to horseradish peroxidase) incubation (RT) were carried out. Amersham ImageQuant™ 800 Western Blot Imaging was utilized to detect chemiluminescence signal from the ECL–treated nylon membrane (Western Lightning® Plus-ECL), in an exposure interval of 25 minutes. For dot intensity analysis, ImageJ was employed.

Results

In order to test whether C/EBPβ isoform expression is dictated by $m^6A_{(m)}$ modulation, we made use of triple negative breast cancer (TNBC) and luminal A breast cancer cell lines. Previous evidence from our lab showed that C/EBPβ-LIP promoted invasion and migration, which paved the way to demonstrating that C/EBPβ understanding in the context of breast cancer is relevant (Sterken et al., 2022). Complementary, recent data suggests that dysregulated m^6A modulation takes place in several cancers (Han & Choe, 2020). All things considered, the study of C/EBPβ's epitranscriptomic regulation in breast cancer cell lines not only does it allow us to elucidate its regulatory effect on C/EBPβ's isoform expression but it can also provide with new insights for breast cancer treatment opportunities. Confirmation of either OE or KD of METTL3, METTL14, WTAP, FTO or ALKBH5 was successful at the RNA level, except for METTL14 in the BT20 cell line (**Suppl. Figs. 1a–e**).

Modulation of $m^6A_{(m)}$ players does not result in changes in CEBPB *mRNA content*

As aforementioned, epitranscriptomic marks such as m^6A have been described to impact both the stability and translation of transcripts by affecting RNA secondary structure perturbation or regulation of RNA-binding motifs (Roundtree et al., 2017; Frye et al., 2018). Because of this, we set out to determine the RNA levels of *CEBPB* upon $m^6A_{(m)}$-modulating protein changes, in aims of finding out whether the *CEBPB* transcript's stability and/or half-life depends on adenosine methylation decoration (**Fig. 3**). While it is clear that all three cell lines (BT20, MDA-MB-231 and MCF-7) displayed varying *CEBPB* levels upon overexpression (OE) or knock-down (KD) of $m^6A_{(m)}$ players, an interesting trend of increased *CEBPB* mRNA expression is seen upon KD of the demethylases ALKBH5 and FTO; as well as a drop upon METTL3 KD. These results are contrary to previous observations that m^6A-decorated transcripts display shorter half-lives, as METTL3 KO cells were seen to present mRNAs with at least two times longer half-lives (Ke et al., 2017). In the present study, C/EBPβ mRNA seems to be regulated in the opposite way. Notably, total mRNA content does not directly reflect features like transcript stability or half-life. Therefore, further observations that measure parameters such as mRNA decay rate are necessary (Chen et al., 2008). All in all, alteration of $m^6A_{(m)}$ methyltransferases or demethylases does not seem to have a strong effect in the *CEBPB* transcript content.

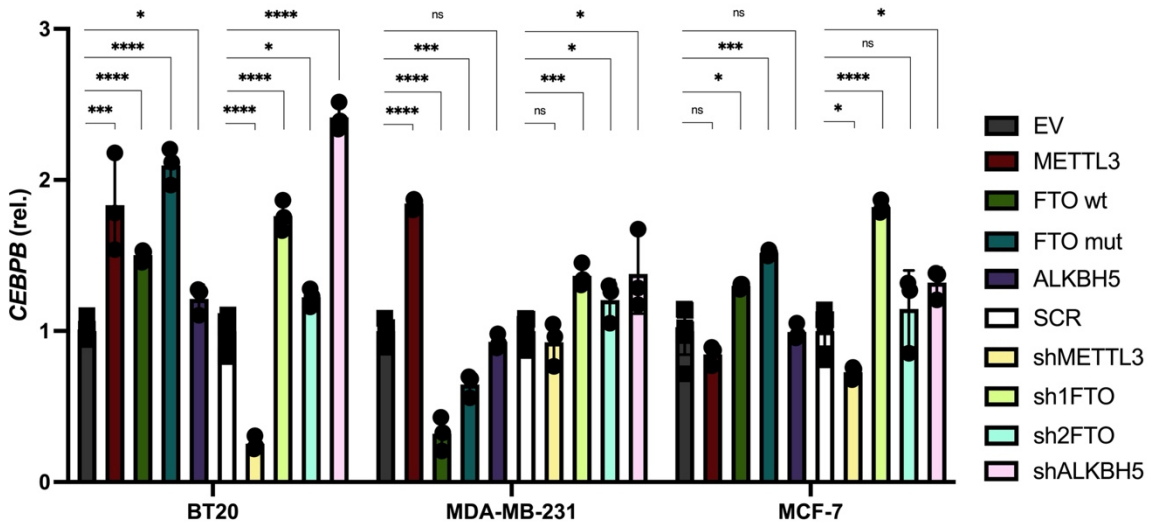

Figure 3. *CEBPB* transcript content. Cell lines BT20, MDA-MB-231 and MCF-7 were used to overexpress or knock-down selected proteins. While a modest increase after KD of FTO/ALKBH5 is observed, complementary to a decrease in *CEBPB* after METTL3 KD, $m^6A_{(m)}$ player modulation does not appear to harbor consistent effects on the total content of *CEBPB* transcript. *EV*: empty vector control; *SCR*: scrambled shRNA. Statistical analysis was performed with multiple Student's independent t-test. *: p<0.05, **: p<0.01, ***: p<0.001, ****: p<0.0001, ns: not significant. Technical replicates are represented with squares (controls) or dots.

The methyltransferase complex displays mild effects on either the C/EBPβ–LIP:LAP ratio or the total C/EBPβ protein content

Taking into account that m^{6}A-mediated uORF translation re-initiation events have been described upon modulation of players of the multi-subunit methyltransferase complex in the ATF4 gene (Zhou et al., 2018), and evidence pointing to *CEBPB* harboring m^{6}A modifications (Linder et al., 2015; Sun et al., 2021; Ben-Haim et al., 2021), we overexpressed and knocked-down METTL3, WTAP and METTL14 in BT20, MDA-MB-231 and MCF-7 cell lines.

METTL3 OE/KD

Since METTL3 harbors the catalytically active site, we tested the effect of its overexpression or knock-down on the C/EBPβ–LIP:LAP ratio. Our results, despite consisting on single biological replicates, indicate that METTL3 OE or KD has no consistent effect on C/EBPβ's isoforms ratio (**Figs. 4a, 4b**). C/EBPβ's total protein content tended to be higher in the METTL3 overexpressing cells but also in BT20 and MDA-MB-231 cells with METTL3 knock-down (**Fig. 4c**), which interestingly differs to what was observed at the RNA level (**Fig. 3**). Importantly, METTL3 OE yielded unphysiologically high METTL3 RNA and protein levels (especially in MDA-MB-231 and MCF-7 cell lines), which might indicate that results in these cell lines are not biologically accurate.

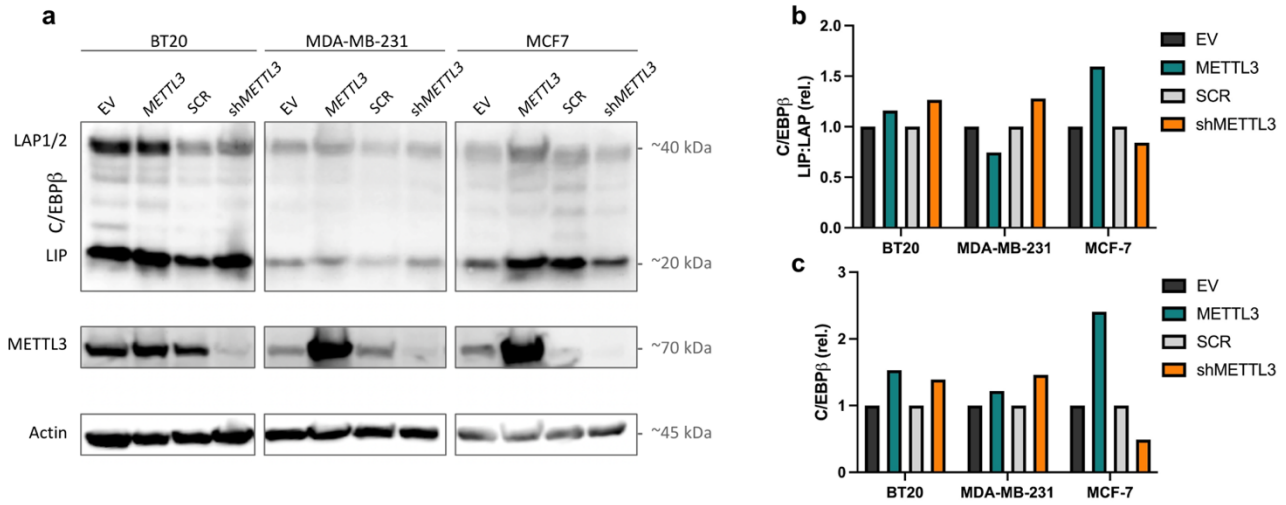

Figure 4. Protein analysis of METTL3 overexpression and knock-down. a| Immunoblot of METTL3 OE/KD of BT20, MDA-MB-231 and MCF-7 cell lines. β-actin served as loading control. **b**| Immunoblot quantification of C/EBPβ–LIP:LAP ratio showing no apparent effect in response to METTL3 overexpression or knock-down. **c**| Immunoblot quantification of total C/EBPβ protein content, which manifests increased C/EBPβ under all conditions except for METTL3 KD in MCF-7 cells. Total C/EBPβ was normalized to β-actin.

WTAP OE/KD

Based on observations that WTAP KD increased the C/EBPβ–LIP:LAP ratio in two triple-negative breast cancer (TNBC) cell lines (Zuidhof et al., 2022-B), we replicated and complimented these results by including WTAP-overexpressed cell lines (**Fig. 5a**). Indeed, WTAP KD only resulted in an increase in the LIP:LAP ratio in BT20 and MCF7 cells, but not in MDA-MB-231 cells. (**Fig. 5b**), whereas WTAP OE showed a slight reduction in the LIP:LAP ratio in BT20 and MDA-MB-231 cell lines, but an increase in MCF-7. A marked increase was seen in the total C/EBPβ protein content in OE cell lines (**Fig. 5c**), which could be inferred to result from increased levels of C/EBPβ–LAP (**Suppl. Fig. 2**). An unclear effect on total C/EBPβ was observed in WTAP KD cell lines. Contrary to METTL3's pLVX-IRES-neo^R–mediated infection, WTAP overexpression levels were somewhat more modest, allowing for a more trustworthy interpretation of the results.

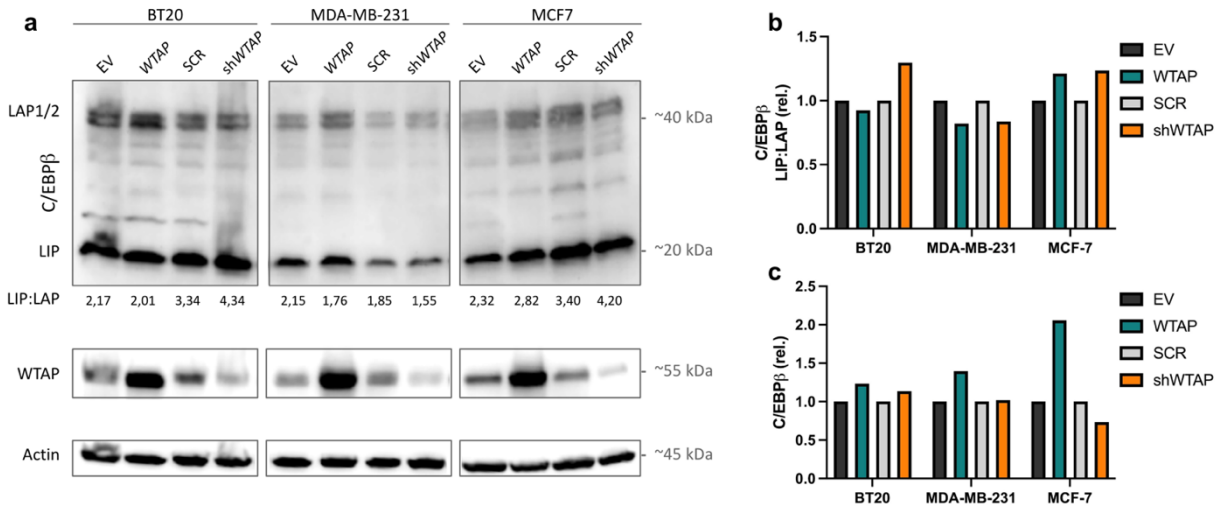

Figure 5. Protein analysis of WTAP overexpression and knock-down. a| Immunoblot of WTAP OE/KD of BT20, MDA-MB-231 and MCF-7 cell lines. β-actin served as loading control. **b**| Immunoblot quantification of C/EBPβ–LIP:LAP ratio. WTAP is seen to generally decrease the LIP:LAP ratio, and vice versa. **c**| Immunoblot quantification of total C/EBPβ protein content, which is seen to increase substantially upon WTAP OE and remain fairly unchanged after KD. Total C/EBPβ was normalized to β-actin.

METTL14 OE/KD

Data from overexpression or knock-down of METTL14, the RNA-binding subunit of the methyltransferase complex, indicated no differences in the C/EBPβ–LIP:LAP ratio (**Figs. 6a, 6b**). Complementary to WTAP, a noticeable increase in total C/EBPβ protein levels can generally be observed in METTL14-overexpressed cells, opposite to what is mainly seen in KD cell lines (**Fig. 6c**). Nonetheless, these results were not exempt from technical difficulties. Sonication of the samples was unsuccessful on the first try (data not shown), and transfer membrane shortage took place consecutively on a second try. Protein detection to confirm METTL14 was unsuccessful, so confirmation of OE/KD was done at the RNA level alone (**Suppl. Fig. 1b**). Little sample amount impeded repetition of such assay. Therefore, further repetition of the experiment should confirm whether or not alteration of METTL14 changes either C/EBPβ isoform expression or total content.

Demethylases FTO and ALKBH5 show opposing effects on the C/EBPβ–LIP:LAP ratio

Taking into account mTORC1's role in stimulating LIP translation, several studies have described induction of S6 kinase 1 (S6K1) phosphorylation upon FTO overexpression, and vice versa (Wang et al., 2017; Li et al., 2018; Yang et al., 2019). These results represent a drawback in the interpretation of results stemming from FTO's modulation, despite the effect of the mTORC1 signaling pathway on C/EBPβ isoform expression not being tested in the present study. Conversely, data surrounding ALKBH5's effect on mTORC1's downstream phosphorylation events appear to have contrary effects in different studies, either by promoting activation of AKT or by reducing PTEN protein expression (Li et al., 2021-A; Li et al., 2021-B). On this matter, the overall effect of these demethylases on the C/EBPβ–LIP:LAP ratio and total C/EBPβ, and, in addition on phosphorylation of S6K1 as a readout of mTORC1 activity are assessed in this chapter. As aforementioned, confirmation of either FTO OE or KD was successful at the RNA level (**Suppl. Figs. 1d, 1e**).

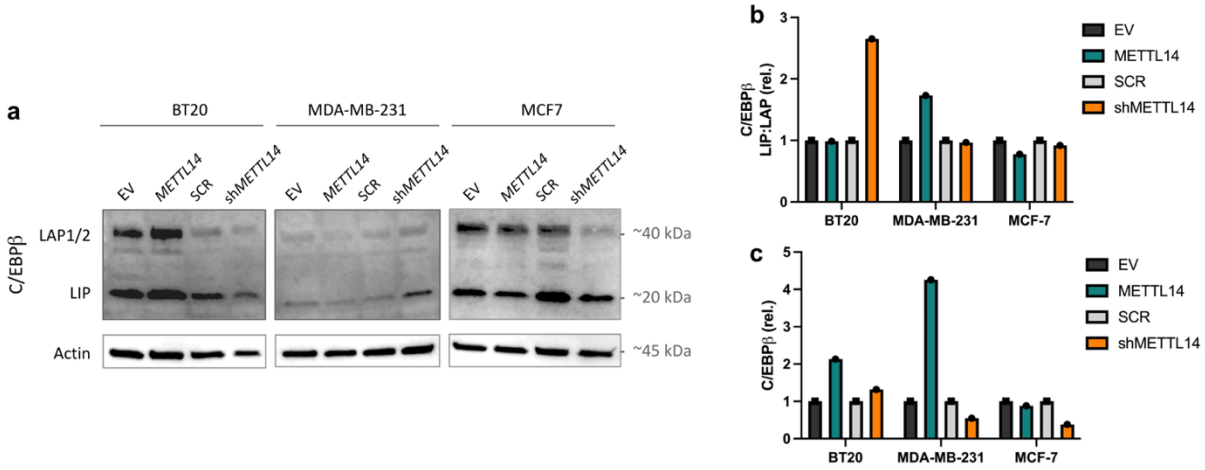

Figure 6. Protein analysis of METTL14 overexpression and knock-down. a| Immunoblot of METTL14 OE/KD of BT20, MDA-MB-231 and MCF-7 cell lines. β-actin served as loading control. **b**| Immunoblot quantification of C/EBPβ–LIP:LAP ratio, manifesting inconsistent changes upon METTL14 overexpression and knock-down. **c**| Immunoblot quantification of total C/EBPβ protein content, displaying a marked increase upon METTL14 OE (except in MCF-7s) and a noticeable drop after KD. Total C/EBPβ was normalized to β-actin.

ALKBH5 OE/KD

The m^6A-strictly demethylase ALKBH5 can be a key factor for determining differences between m^6A- and m^6A_m-mediated effects on transcript modification, since it has no catalytic activity towards m^6A_m (Shi et al., 2019). ALKBH5 modulation consistently demonstrated reduced C/EBPβ–LIP:LAP ratios upon ALKBH5 OE and increased ratios upon ALKBH5 KD, without apparent changes in the total C/EBPβ content (**Fig. 7a, 7b, 7c**). Considering the contradictory data revolving around its effect on the mTORC1 pathway, and the lack of previous literature on the effect on downstream mTORC1's effectors, we demonstrated a clear implication of ALKBH5 on S6K1 phosphorylation in the MCF-7 cell line. The mTORC1 complex is a signaling hub that

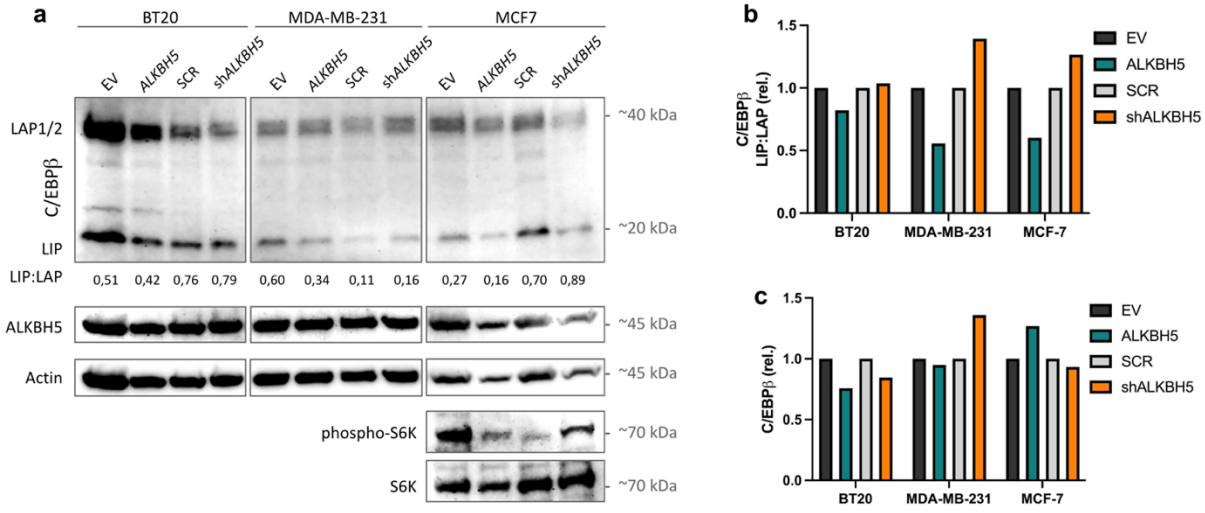

Figure 7. Protein analysis of ALKBH5 overexpression and knock-down. a| Immunoblot of ALKBH5 OE/KD of BT20, MDA-MB-231 and MCF-7 cell lines. β-actin served as loading control. **b**| Immunoblot quantification of C/EBPβ–LIP:LAP ratio, which manifest a clear reduction in all ALKBH5-overexpressing cell lines and a LIP:LAP ratio reduction after ALKBH5 KD. **c**| Immunoblot quantification of total C/EBPβ protein content displaying no apparent changes upon ALKBH5 modulation. Total C/EBPβ was normalized to β-actin.

essentially carries out its downstream functions through phosphorylation of target proteins like S6K1 or 4EBP. From a technical point of view, assessment of this phosphorylation state reflects a measure of mTORC1 activation (Ben-Sahra & Manning, 2017). These results might indicate that the observed effect on the LIP:LAP ratio might not reflect a direct measure of ALKBH5-targeted demethylation of the *CEBPB* transcript but rather result from indirect consequences like altered mTORC1 activity. Due to undetermined motives, ALKBH5 itself did not reflect any change at its protein level, although the *ALKBH5*'s RNA levels clearly showed the expected changes (**Suppl. Fig. 1d**). Whether this shows that ALKBH5 protein levels are stable regardless of RNA transcripts is unknown, but efforts to OE or KD ALKBH5 have been successfully described at the protein level (Zhang et al., 2020).

FTO OE/KD

Taking into account that prior observations showed a decrease in the C/EBPβ–LIP:LAP ratio upon FTO KD (Zuidhof et al., 2022-B), we opted for validation of these results in three different cell lines (**Fig. 8a**). Indeed, a reduced LIP:LAP ratio was found upon every cell line and FTO specific shRNA, except for the case of BT20 (**Fig. 8b**), which was already previously seen to remain unchanged after FTO KD (sh1FTO) (Zuidhof et al., 2022-B).

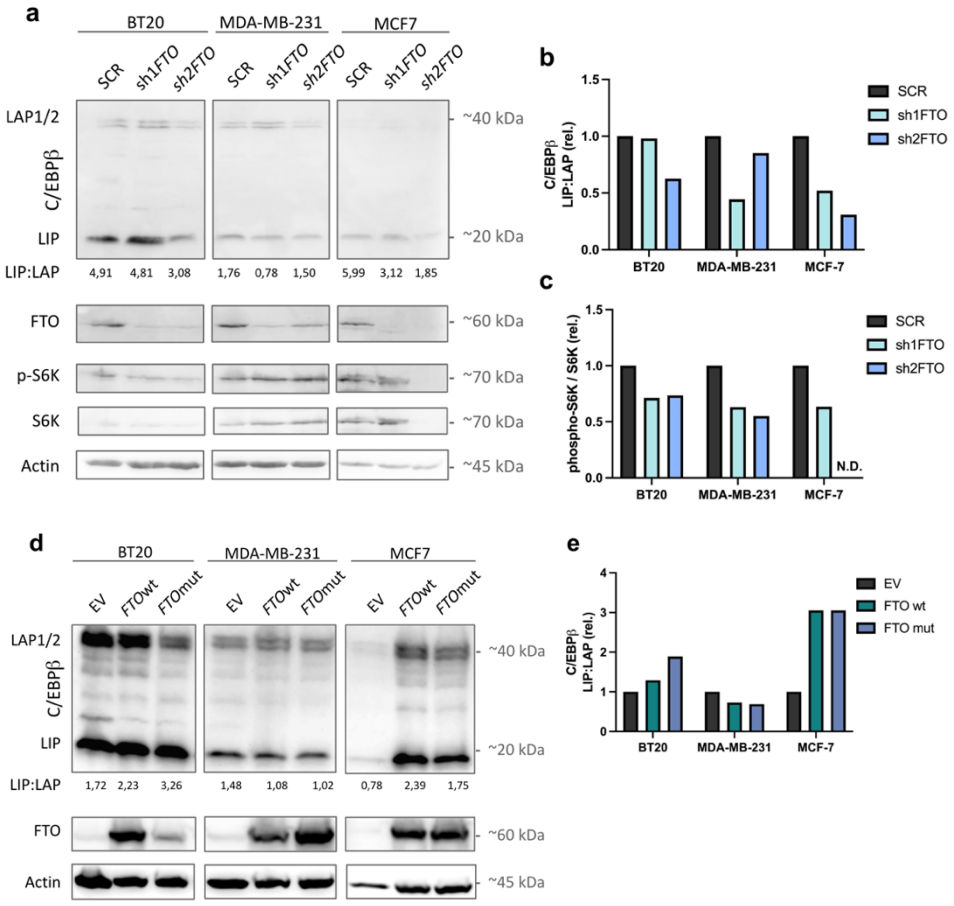

Figure 8. Protein analysis of FTO knock-down and overexpression. a| Immunoblot of FTO KD of BT20, MDA-MB-231 and MCF-7 cell lines. β-actin served as loading control. **b**| Immunoblot quantification of C/EBPβ–LIP:LAP ratio in FTO KD cell lines. An evident decrease of such ratio can be observed. **c**| Immunoblot quantification of S6K1 phosphorylation ratio in FTO KD cell lines, demonstrating that FTO KD reduces S6K1 phosphorylation. **d**| Immunoblot of FTO OE of BT20, MDA-MB-231 and MCF-7 cell lines. β-actin served as loading control. **e**| Immunoblot quantification of FTO OE C/EBPβ–LIP:LAP ratio, which had the tendency to appear increased. *N.D.*: non-detectable.

Notwithstanding, protein quantification of S6K1 and its phosphorylated counterpart demonstrated a reduced S6K1 phosphorylation ratio upon FTO KD. Once again, the reduction of the C/EBPβ–LIP:LAP ratio after FTO KD could well be explained through decreased mTORC1 signaling (**Fig. 8c**), ultimately reducing LIP translation. These results might once more indicate that such effect on the LIP:LAP ratio may not reflect a direct measure of FTO-targeted demethylation of the *CEBPB* transcript.

On the other hand, overexpression of either FTO wild-type (FTO wt) or its catalytically mutant equivalent (FTO mut) increased the LIP:LAP ratio in BT20 and MCF-7 but not MDA-MB-231 (**Figs. 8d, 8e**). Moreover, both FTO forms displayed a propensity to behaving in a similar way, despite prior description of FTO's R316Q mutant displaying decreased demethylation activity (Boissel et al., 2009; Daoud et al., 2016). Due to time constraints, replication of the experiment was not performed, and phosphorylation of S6K1 was not assessed (could not be detected in the membrane shown, due to the strong expression signal of FTO). Data from FTO's OE in MCF-7 should be interpreted with caution as protein loading was lower in the EV control.

Interestingly, total C/EBPβ protein content was seen to generally increase upon sh1FTO and decrease after sh2FTO infection; and it was also markedly increased upon FTO wt induction with either milder or no effects with the mutant FTO construct (**Suppl. Fig. 3**). A further global methylation assay showed unclear differences between the mutant construct and the wild-type, or even between KD and OE FTO conditions, probably due to low total mRNA spotting and irregular background signal (**Suppl. Fig. 4**). These data indicate that either *CEBPB* transcript stability or half-life and/or C/EBPβ translation could partially be governed by $m^6A_{(m)}$ regulation. Understanding why both shRNAs against FTO might have different effects on C/EBPβ's resulting protein levels could also shed new light on FTO's $m^6A_{(m)}$ demethylating effects on *CEBPB*, and, consequently, C/EBPβ biology.

FTO inhibition results in the reduction of the C/EBPβ–LIP:LAP ratio, associated with a decrease in mTORC1 signaling

Entacapone was discovered to be an FTO inhibitor through a hierarchical virtual screening, and later confirmed to display a median inhibitory concentration of 3.5 μM towards FTO (Peng et al., 2019). Based on these findings, we treated cell lines BT20, MDA-MB-231 and MCF-7 with either 10 μM or 50 μM entacapone (in DMSO) for 72h. As in the case for FTO KD, a marked and dose-dependent decrease of the LIP:LAP ratio was consistently observed in all three cell lines (**Fig. 9a, 9b**). mTORC1 activation was once again assessed by S6K1 phosphorylation, which resulted to be decreased (**Fig. 9c**). FTO inhibition yielded no changes in the C/EBPβ–LIP:LAP ratio after 24 or 48h of entacapone treatment, except for MCF-7s after 48h (**Suppl. Fig. 5**). Altogether, these results suggest that such decrease in the LIP:LAP ratio could be explained by reduced mTORC1 signaling.

ALKBH5 OE mediates a two-fold increase in C/EBPβ protein content in FTO-depleted cell clones

In aims of replicating the results seen in FTO KD cell lines on the C/EBPβ–LIP:LAP ratio, we made use of CRISPR/Cas9–generated MDA-MB-231 FTO knock-out (KO) clones. Residual expression of any protein (i.e., KD) can yield different results than its complete elimination (i.e., KO). For example, little amount of protein can be sufficient to supply with its function(s), the corresponding shRNA may have off-target effects on the genome or non-coding RNA species included within the gene's sequence in intronic regions can end up being wiped off (i.e., KO). Additionally, genetic compensation can also play a role in showing differential results between KD and KO cell lines or organisms (El-Brolosy & Stainier, 2017). To elucidate this, we characterized the C/EBPβ–

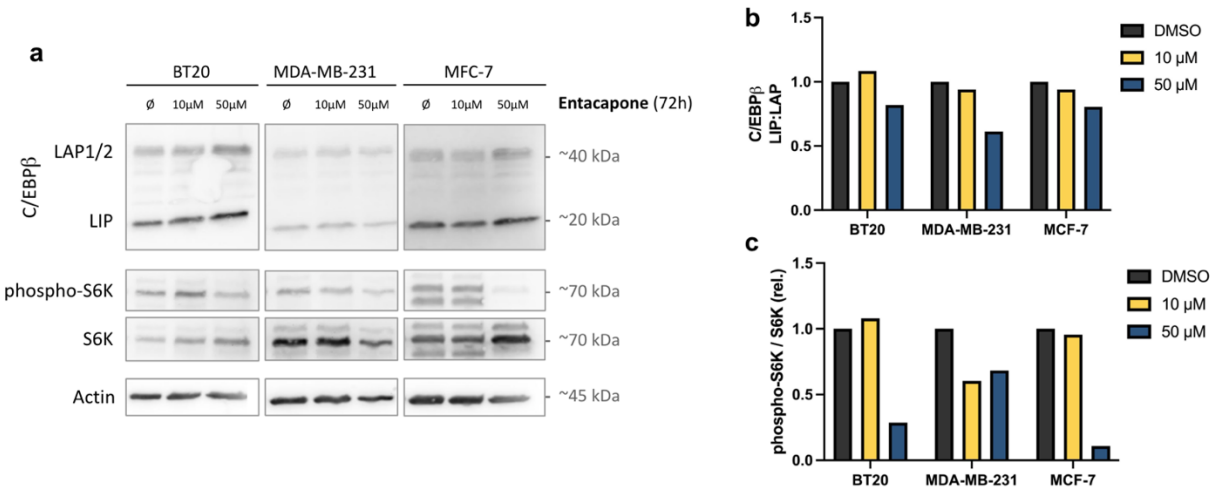

Figure 9. Protein analysis of entacapone-treated cell lines. a| Immunoblot of FTO inhibited BT20, MDA-MB-231 and MCF-7 cell lines after 72h. β-actin served as loading control. **b**| Immunoblot quantification of entacapone-mediated C/EBPβ–LIP:LAP ratio, which is reduced in a dose-dependent manner. **c**| Immunoblot quantification of entacapone-mediated reduced S6K1 phosphorylation.

LIP:LAP ratio of MDA-MB-231 FTO KO clones and overexpressed $m^6A_{(m)}$ demethylases to bring back their function.

MDA-MB-231 FTO KO C/EBPβ characterization

In order to confirm the lack of FTO in three different MDA-MB-231 FTO KO clones we immunoblotted FTO in these clones with a wild-type control MDA-MB-231 cell line. As expected, no FTO could be detected in neither of the three clones (**Fig. 10a**). Notwithstanding, in none of the two experimental rounds was there a consistent effect on the C/EBPβ–LIP:LAP ratio; yet total C/EBPβ was strikingly lower compared to the wild-type counterpart (data from the first not shown) (**Figs. 10b, 10c**). These data might indicate that the total C/EBPβ levels, but not the LIP:LAP ratio, are governed by FTO.

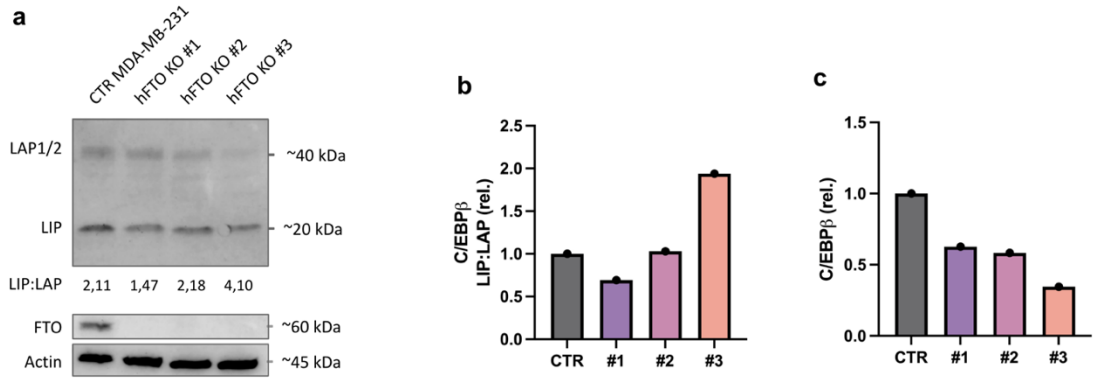

Figure 10. Protein analysis of FTO KO MDA-MB-231 clones #1, #2 & #3. a| Immunoblot of FTO KO MDA-MB-231 cell clones with wild-type MDA-MB-231 cell line as biological control. β-actin served as loading control. **b**| Immunoblot quantification of the C/EBPβ–LIP:LAP ratio, manifesting no consistent changes. **c**| Immunoblot quantification of total C/EBPβ protein content, clearly showing that MDA-MB-231 FTO KO cells harbor less C/EBPβ. Total C/EBPβ was normalized to β-actin.

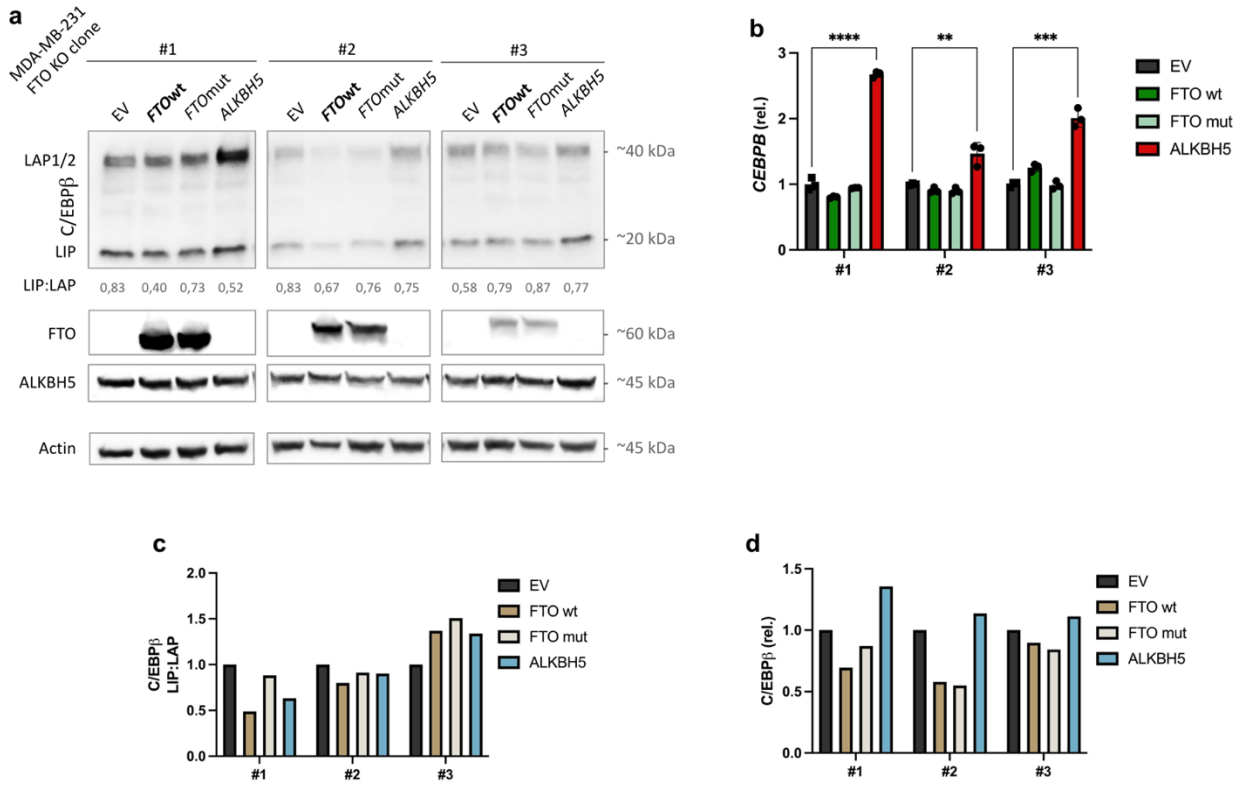

Figure 11. Protein and RNA analysis of FTO/ALKBH5-OE MDA-MB-231 FTO KO clones #1, #2 & #3. a| Immunoblot of FTO KO MDA-MB-231 cell clones overexpressed with either FTO wt, FTO mut or ALKBH5. β-actin served as loading control. **b**| RT-qPCR RNA quantification of total *CEBPB* content. A clear increase in *CEBPB* is observed upon ALKBH5 OE. Statistical significance was determined by unpaired Student's t test. **: p<0.01, ***: p<0.001, ****: p<0.0001 **c**| Immunoblot quantification of the C/EBPβ–LIP:LAP ratio, with no consistent changes. **d**| Immunoblot quantification of total C/EBPβ protein content. A clear increase in C/EBPβ protein content is observed upon ALKBH5 OE. Total C/EBPβ was normalized to β-actin.

Overexpression of ALKBH5 rescues low C/EBPβ protein content in the MDA-MB-231 FTO KO cell line

We then set out to infect MDA-MB-231 FTO KO clones with FTO wt, FTO mut and ALKBH5 cloned in a pLVX-IRES-neo^R backbone. Since such clones already contain ALKBH5, this RNA demethylase was included in means of controlling the effect of m^6A over m^6A_m, given that FTO's true target is controversial in the epitranscriptomic field (Mauer et al., 2017; Ben-Haim et al., 2021). RT-qPCR of either *FTO* or *ALKBH5* confirmed their OE status at the RNA level (**Suppl. Fig. 6a, 6b**). Peculiarly, total *CEBPB* transcript quantification showed a two-fold increase upon ALKBH5 overexpression, which was not apparent following FTO replenishment (**Fig. 11b**). Complementary, protein analysis showed more elevated C/EBPβ levels in the ALKBH5-overexpressing clones, yet lower C/EBPβ content in the FTO-rescued FTO KO MDA-MB-231 cell lines (**Figs. 11a, 11d**). Moreover, the C/EBPβ–LIP:LAP ratio appeared to show no differences in these conditions, but a trend of FTO-mutant infected cells having the highest LIP:LAP ratio out of the other constructs was observed (**Fig. 11c**). All in all, these results point towards the understanding that FTO-mediated effects on C/EBPβ isoform expression might not reflect a direct effect of *CEBPB*'s demethylation, since (1) no differences are seen in C/EBPβ–LIP:LAP ratios in MDA-MB-231 FTO KO cells and (2) rescue of FTO does not show any consistent change in its isoform expression levels.

Discussion

The epitranscriptome is described to provide a dynamic layer of transcript control that is malleable among different states, tissues or stimuli (Ben-Haim et al., 2021). Due to its (increasing) complexity, it is no wonder that such a tightly-regulated feature of RNA biology can have decisive effects on gene expression, and data arising from its study are sure to shed new light on non-understood facets of transcript control. In the present work, we elucidated the effect of altering the expression of several proteins implicated in the $m^6A_{(m)}$ methylome on C/EBPβ's isoform expression.

Here, we describe how the multi-subunit N^6-methylating (m^6A) writing complex (METTL3,14-WTAP) increases C/EBPβ protein content, with players like WTAP having an implication on reducing the C/EBPβ–LIP:LAP ratio. Interestingly, demethylase activity was also linked to alterations in the proportion of isoforms in an mTORC1 associated context: while the reduced function of FTO (upon knock-down or pharmacological inhibition) was seen to reduce S6K1 phosphorylation in parallel with the LIP:LAP ratio; ALKHB5 displayed the contrary effect. As previously described, mTORC1 stimulates C/EBPβ–LIP translation (Calkhoven et al., 2000). Whether mTORC1 is the sole reason for such alteration of the C/EBPβ–LIP:LAP isoform ratio is unknown, since FTO's or ALKBH5's effect in an mTORC1-inhibited context was not tested. Complementary, FTO KO cells appear to harbor reduced C/EBPβ content, which can be rescued with ALKBH5 but not FTO.

As is certain, evidence pointing to an $m^6A_{(m)}$-mediated direct effect on C/EBPβ's isoform expression is still inconclusive: demethylase activity from FTO or ALKBH5 appears to have opposite effects on the LIP:LAP ratio, results are not always replicated in all cell lines and the effect is not always seen to be reverted in opposing conditions (KD vs. OE). This is further complicated by the fact that mTORC1 signaling has recently been described to stimulate m^6A mRNA methylation through enhanced WTAP expression and/or translation (Cho et al., 2021; Villa et al., 2021; Tang et al., 2021). On top of this, mTORC1 has also been seen to enhance methyltransferase function by promoting the production of S-adenosylmethionine, the universal methyl group donor (Villa et al., 2021). In this scenario, mTORC1-modulating proteins could ultimately promote differential m^6A writing through the action of WTAP, aside from their intrinsic functions. Taking into account that in the present study WTAP KD increased the C/EBPβ–LIP:LAP ratio, these findings do not fit to our observations of why ALKBH5's inhibiting effects on mTORC1 do not result in such increase, or neither why FTO KD promotes a low LIP:LAP ratio. Complementary, having WTAP's-associated C/EBPβ protein increase in mind, mTORC1-activating proteins like FTO should also be expected to exhibit higher C/EBPβ levels, which is partially replicated in our work. Nonetheless, ALKBH5 showed no apparent changes in C/EBPβ content. Taken together, these results leave us to question whether mTORC1 contributes to C/EBPβ's isoform expression more efficiently through eIF-4E induction (Calkhoven et al., 2000) or through its WTAP-mediated effects. To untangle this, the effect on C/EBPβ–LIP:LAP ratio should be also assessed in an mTORC1–activated context in WTAP KD/KO cells.

In addition, it is also striking how similarly the wild-type FTO and the catalytically-impaired FTO mutant behaved, despite sequencing results corroborating two G to A transitions resulting in arginine to glutamine missense mutations (R316.322Q) in the mutant form of FTO. Boissel and colleagues identified the R316Q FTO mutation (in homozygosis) in a family that presented serious growth retardation and facial dysmorphism, among others. This mutation was regarded to render FTO unable of harboring residual catalytic activity (Boissel et al., 2009). A further FTO mutation was described, S319F, which was seen to be consistent with causing a reduced enzymatic activity in FTO (Daoud et al., 2016). Whether the R316.322Q missense mutation truly depletes FTO from executing its function was not tested in the present work, but our data point towards the understanding that under high overexpression conditions residual catalytic activity is sufficient to restore

its function. In this scenario, it is of the utmost importance to validate in a pan-transcript context if FTO-overexpressed samples actually present less N^6-methyladenosine–containing RNA than those containing the mutated FTO. Due to technical difficulties, this could not be objectively demonstrated in the present work and further mRNA methylation data are required. Complementary, FTO bearing functions independent from its $m^6A_{(m)}$ demethylase could also explain the similarity of results of the catalytically impaired FTO and the wild-type counterpart. Recently, FTO was described to be a WNT signaling pathway regulator through the action of the WNT inhibitor DKK1 (independently of its demethylase activity), the transcript of which showed no mRNA increased levels and was not over-methylated in an FTO KD context (Kim et al., 2022). While inviting, these results should be considered carefully since the detection limit of the technical assessment could not be reliable enough to detect small changes (like the loss of a single m^6A_m), and no protein pull-down essay to confirm such interaction was performed.

Our data on FTO KO cells suggests that either m^6A or m^6A_m elimination might bear an effect on total C/EBPβ protein content. On the one hand, lack of m^6A is generally understood to have a stabilizing effect on mRNA species (Ke et al., 2017); while on the other, our results on total C/EBPβ content in m^6A-writer-devoid samples do not reflect features of increased stability. For these reasons, it is understandable to think that FTO might modulate *CEBPB* stability and/or turnover by its effects on m^6A_m rather than m^6A. In order to confirm such claims, it would be highly relevant to assess the effect of the m^6A_m cap-specific methyltransferase PCIF1/CAPAM (Boulias et al., 2021) in the tested cell lines, considering that 92% of transcripts starting with an A contain the m^6A_m modification (Akichika et al., 2019). Should *PCIF1* overexpression generate similar results as those seen in FTO KO cell lines, it would confirm that *CEBPB* methylation at the first adenosine adjacent to the cap provides the transcript stability and/or promotes its translation. Notably, *CEBPB* has not been confirmed to be m^6A_m-decorated so far, and evidence on m^6A modifications in its transcript is rather variable across studies (Linder et al., 2015; Sun et al., 2021; Boulias et al., 2021; Ben-Haim et al., 2021; Hu et al., 2022). Data on transcriptome-wide $m^6A_{(m)}$ methylation is scarce, even in non-peer reviewed databases like BioRxiv. In this scenario, it is paramount to fully elucidate *CEBPB*'s methylome profile with $m^6A_{(m)}$ mapping techniques that can distinguish m^6A from m^6A_m modifications like miCLIP (Linder et al., 2015). Sequencing studies using antibody-based detection methods like meRIP-seq/m^6A-seq or LAIC-seq should be taken with caution since these m^6A mapping techniques cannot distinguish m^6A from m^6A_m (Zaccara et al., 2019), labeling potential m^6A_m marks as m^6A peaks at the 5' UTR.

In parallel, our findings in FTO KO cells never covered whether an endogenous ALKBH5-mediated compensatory mechanism took place. In these settings, cells lacking the FTO gene could be forced to induce ALKBH5 transcription and/or translation to make up for the lack of demethylase activity. Should this be confirmed, it would explain why no effect on the C/EBPβ–LIP:LAP ratio was seen in any of the three FTO KO clones: FTO's absence effect could be dampened with higher ALKBH5 content, since they display opposing consequences on C/EBPβ isoform ratio determination. In the same line, restoration of FTO's presence in KO cells by making use of inducible FTO constructs could also unravel many features of gene compensatory mechanisms in the context of $m^6A_{(m)}$. Furthermore, an important aspect to take into account is the high overexpression achieved during the lentiviral infection rounds. While some cell lines ended up with reasonable levels of overexpression (presenting a 5- to 10-fold increase), others contained as high as 150 times more protein than the corresponding controls (i.e., METTL3 in the MCF-7 cell line). Indeed, determining what level of overexpression is physiologically adequate is not straightforward. In this line, it would be necessary to examine the endogenous protein levels of several cell lines to determine by how many orders of magnitude these change. Because the N^6-methyl modification is seen to be regulated by many pathways, excessive

modulation of its players could reflect aberrant transduction networks effects from signaling cascades like TGFβ/SMAD, MAPKs/ERK or even mTORC1 (Jang et al., 2022).

In summary, we hereby report that C/EBPβ is sensitive to alteration of some $m^6A_{(m)}$-epitranscriptomic players. In this work, we conclude that C/EBPβ isoform expression changes upon modulation of WTAP, FTO and ALKBH5, and that its total protein content is also subject to changes in the methyltransferase m^6A writer complex. Whether such effect is direct or not was not assessed in the current study, but our data pave the way for further experiments. Taken together, our results point towards the understanding that certain features of the *CEBPB* transcript are regulated in an epitranscriptome–mediated fashion in breast cancer cell lines. Importantly, this is the case for the increased C/EBPβ–LAP (but not LIP) isoform fraction in WTAP KD cells. Considering the improved health- and lifespan phenotype of $C/EBP\beta^{\Delta uORF}$ mice (which have a low LIP:LAP ratio) (Müller et al., 2018; Müller et al., 2022), these results open an avenue for conjoined research aimed at tackling cancer, metabolic disorders and aging at the same time. Whether the LIP:LAP ratio will become an interesting target is yet to be seen, but its research in the context of the epitranscriptome will surely bring compelling data about the relevance of mRNA regulation.

References

Akichika, S., Hirano, S., Shichino, Y., Suzuki, T., Nishimasu, H., & Ishitani, R. et al. (2019). Cap-specific terminal N 6 -methylation of RNA by an RNA polymerase II–associated methyltransferase. *Science, 363*(6423). https://doi.org/10.1126/science.aav0080

Bégay, V., Baumeier, C., Zimmermann, K., Heuser, A., & Leutz, A. (2018). The C/EBPβ LIP isoform rescues loss of C/EBPβ function in the mouse. *Scientific Reports, 8*(1). https://doi.org/10.1038/s41598-018-26579-y

Bégay, V., Smink, J., Loddenkemper, C., Zimmermann, K., Rudolph, C., & Scheller, M. et al. (2014). Deregulation of the endogenous C/EBPβ LIP isoform predisposes to tumorigenesis. *Journal Of Molecular Medicine, 93*(1), 39-49. https://doi.org/10.1007/s00109-014-1215-5

Ben-Haim, M., Pinto, Y., Moshitch-Moshkovitz, S., Hershkovitz, V., Kol, N., & Diamant-Levi, T. et al. (2021). Dynamic regulation of N6,2'-O-dimethyladenosine (m6Am) in obesity. *Nature Communications, 12*(1). https://doi.org/10.1038/s41467-021-27421-2

Ben-Sahra, I., & Manning, B. (2017). mTORC1 signaling and the metabolic control of cell growth. *Current Opinion In Cell Biology, 45*, 72-82. https://doi.org/10.1016/j.ceb.2017.02.012

Boissel, S., Reish, O., Proulx, K., Kawagoe-Takaki, H., Sedgwick, B., & Yeo, G. et al. (2009). Loss-of-Function Mutation in the Dioxygenase-Encoding FTO Gene Causes Severe Growth Retardation and Multiple Malformations. *The American Journal Of Human Genetics, 85*(1), 106-111. https://doi.org/10.1016/j.ajhg.2009.06.002

Boulias, K., Toczydłowska-Socha, D., Hawley, B., Liberman, N., Takashima, K., & Zaccara, S. et al. (2019). Identification of the m6Am Methyltransferase PCIF1 Reveals the Location and Functions of m6Am in the Transcriptome. *Molecular Cell, 75*(3), 631-643.e8. https://doi.org/10.1016/j.molcel.2019.06.006

Calkhoven, C., Müller, C., & Leutz, A. (2000). Translational control of C/EBPα and C/EBPβ isoform expression. *Genes &Amp; Development, 14*(15), 1920-1932. https://doi.org/10.1101/gad.14.15.1920

Cao, Z., Umek, R., & McKnight, S. (1991). Regulated expression of three C/EBP isoforms during adipose conversion of 3T3-L1 cells. *Genes &Amp; Development, 5*(9), 1538-1552. https://doi.org/10.1101/gad.5.9.1538

Chen, C., Ezzeddine, N., & Shyu, A. (2008). Chapter 17 Messenger RNA Half-Life Measurements in Mammalian Cells. *Methods In Enzymology*, 335-357. https://doi.org/10.1016/s0076-6879(08)02617-7

Chiu, C., Lin, W., Huang, S., & Lee, Y. (2004). Effect of a C/EBP gene replacement on mitochondrial biogenesis in fat cells. *Genes &Amp; Development, 18*(16), 1970-1975. https://doi.org/10.1101/gad.1213104

Cho, S., Lee, G., Pickering, B., Jang, C., Park, J., & He, L. et al. (2021). mTORC1 promotes cell growth via m6A-dependent mRNA degradation. *Molecular Cell, 81*(10), 2064-2075.e8. https://doi.org/10.1016/j.molcel.2021.03.010

Cohn WE, Volkin E. (1951). Nucleoside-5'-phosphates from ribonucleic acid. *Nature 167*, 483-4; http://dx.doi.org/10.1038/167483a0

Daoud, H., Zhang, D., McMurray, F., Yu, A., Luco, S., & Vanstone, J. et al. (2015). Identification of a pathogenicFTOmutation by next-generation sequencing in a newborn with growth retardation and developmental delay. *Journal Of Medical Genetics, 53*(3), 200-207. https://doi.org/10.1136/jmedgenet-2015-103399

Descombes, P., & Schibler, U. (1991). A liver-enriched transcriptional activator protein, LAP, and a transcriptional inhibitory protein, LIP, are translated from the sam mRNA. *Cell, 67*(3), 569-579. https://doi.org/10.1016/0092-8674(91)90531-3

Dominissini, D., Moshitch-Moshkovitz, S., Schwartz, S., Salmon-Divon, M., Ungar, L., & Osenberg, S. et al. (2012). Topology of the human and mouse m6A RNA methylomes revealed by m6A-seq. *Nature, 485*(7397), 201-206. https://doi.org/10.1038/nature11112

El-Brolosy, M., & Stainier, D. (2017). Genetic compensation: A phenomenon in search of mechanisms. *PLOS Genetics, 13*(7), e1006780. https://doi.org/10.1371/journal.pgen.1006780

Frayling, T., Timpson, N., Weedon, M., Zeggini, E., Freathy, R., & Lindgren, C. et al. (2007). A Common Variant in the FTO Gene Is Associated with Body Mass Index and Predisposes to Childhood and Adult Obesity. *Science, 316*(5826), 889-894. https://doi.org/10.1126/science.1141634

Frye, M., Harada, B., Behm, M., & He, C. (2018). RNA modifications modulate gene expression during development. *Science, 361*(6409), 1346-1349. https://doi.org/10.1126/science.aau1646

Gems, D., & de Magalhães, J. (2021). The hoverfly and the wasp: A critique of the hallmarks of aging as a paradigm. *Ageing Research Reviews, 70*, 101407. https://doi.org/10.1016/j.arr.2021.101407

Han, S., & Choe, J. (2020). Diverse molecular functions of m6A mRNA modification in cancer. *Experimental &Amp; Molecular Medicine, 52*(5), 738-749. https://doi.org/10.1038/s12276-020-0432-y

Hu, L., Liu, S., Peng, Y., Ge, R., Su, R., & Senevirathne, C. et al. (2022). m6A RNA modifications are measured at single-base resolution across the mammalian transcriptome. *Nature Biotechnology*. https://doi.org/10.1038/s41587-022-01243-z

Huang, H., Weng, H., Sun, W., Qin, X., Shi, H., & Wu, H. et al. (2018). Recognition of RNA N6-methyladenosine by IGF2BP proteins enhances mRNA stability and translation. *Nature Cell Biology, 20*(3), 285-295. https://doi.org/10.1038/s41556-018-0045-z

Jang, K., Heras, C., & Lee, G. (2022). m6A in the Signal Transduction Network. *Molecules And Cells, 45*(7), 435-443. https://doi.org/10.14348/molcells.2022.0017

Johnson, S., Rabinovitch, P., & Kaeberlein, M. (2013). mTOR is a key modulator of ageing and age-related disease. *Nature, 493*(7432), 338-345. https://doi.org/10.1038/nature11861

Jundt, F., Raetzel, N., Müller, C., Calkhoven, C., Kley, K., & Mathas, S. et al. (2005). A rapamycin derivative (everolimus) controls proliferation through down-regulation of truncated CCAAT enhancer binding protein β and NF-κB activity in Hodgkin and anaplastic large cell lymphomas. *Blood, 106*(5), 1801-1807. https://doi.org/10.1182/blood-2004-11-4513

Ke, S., Pandya-Jones, A., Saito, Y., Fak, J., Vågbø, C., & Geula, S. et al. (2017). m6A mRNA modifications are deposited in nascent pre-mRNA and are not required for splicing but do specify cytoplasmic turnover. *Genes &Amp; Development, 31*(10), 990-1006. https://doi.org/10.1101/gad.301036.117

Kim, H., Jang, S., & Lee, Y. (2022). The m6A(m)-independent role of FTO in regulating WNT signaling pathways. *Life Science Alliance, 5*(5), e202101250. https://doi.org/10.26508/lsa.202101250

Koh, C., Goh, Y., & Goh, W. (2019). Atlas of quantitative single-base-resolution N6-methyl-adenine methylomes. *Nature Communications, 10*(1). https://doi.org/10.1038/s41467-019-13561-z

Kozak, M. (1987). An analysis of 5'-noncoding sequences from 699 vertebrate messenger RNAs. *Nucleic Acids Research, 15*(20), 8125-8148. https://doi.org/10.1093/nar/15.20.8125

Kretschmer, J., Rao, H., Hackert, P., Sloan, K., Höbartner, C., & Bohnsack, M. (2018). The m6A reader protein YTHDC2 interacts with the small ribosomal subunit and the 5′–3′ exoribonuclease XRN1. *RNA, 24*(10), 1339-1350. https://doi.org/10.1261/rna.064238.117

Lekstrom-Himes, J., & Xanthopoulos, K. (1998). Biological Role of the CCAAT/Enhancer-binding Protein Family of Transcription Factors. *Journal Of Biological Chemistry, 273*(44), 28545-28548. https://doi.org/10.1074/jbc.273.44.28545

Li, H., Ren, Y., Mao, K., Hua, F., Yang, Y., & Wei, N. et al. (2018). FTO is involved in Alzheimer's disease by targeting TSC1-mTOR-Tau signaling. *Biochemical And Biophysical Research Communications, 498*(1), 234-239. https://doi.org/10.1016/j.bbrc.2018.02.201

Li, L., Zhou, M., Chen, B., Wang, Q., Pan, S., & Hou, Y. et al. (2021-B). ALKBH5 promotes cadmium-induced transformation of human bronchial epithelial cells by regulating PTEN expression in an m6A-dependent manner. *Ecotoxicology And Environmental Safety*, 224, 112686. https://doi.org/10.1016/j.ecoenv.2021.112686

Li, X., Xiong, X., & Yi, C. (2016). Epitranscriptome sequencing technologies: decoding RNA modifications. *Nature Methods, 14*(1), 23-31. https://doi.org/10.1038/nmeth.4110

Li, Z., Wang, P., Li, J., Xie, Z., Cen, S., & Li, M. et al. (2021-A). The N6-methyladenosine demethylase ALKBH5 negatively regulates the osteogenic differentiation of mesenchymal stem cells through PRMT6. *Cell Death &Amp; Disease, 12*(6). https://doi.org/10.1038/s41419-021-03869-4

Linder, B., Grozhik, A., Olarerin-George, A., Meydan, C., Mason, C., & Jaffrey, S. (2015). Single-nucleotide-resolution mapping of m6A and m6Am throughout the transcriptome. *Nature Methods, 12*(8), 767-772. https://doi.org/10.1038/nmeth.3453

Loos, R., & Yeo, G. (2013). The bigger picture of FTO—the first GWAS-identified obesity gene. *Nature Reviews Endocrinology, 10*(1), 51-61. https://doi.org/10.1038/nrendo.2013.227

López-Otín, C., Blasco, M., Partridge, L., Serrano, M., & Kroemer, G. (2013). The Hallmarks of Aging. *Cell, 153*(6), 1194-1217. https://doi.org/10.1016/j.cell.2013.05.039

Maity, A., & Das, B. (2015). N6-methyladenosine modification inmRNA: machinery, function and implications for health and diseases. *The FEBS Journal, 283*(9), 1607-1630. https://doi.org/10.1111/febs.13614

Mauer, J., Luo, X., Blanjoie, A., Jiao, X., Grozhik, A., & Patil, D. et al. (2016). Reversible methylation of m6Am in the 5′ cap controls mRNA stability. *Nature, 541*(7637), 371-375. https://doi.org/10.1038/nature21022

McMahon, M., Forester, C., & Buffenstein, R. (2021). Aging through an epitranscriptomic lens. *Nature Aging, 1*(4), 335-346. https://doi.org/10.1038/s43587-021-00058-y

Meyer, K., Saletore, Y., Zumbo, P., Elemento, O., Mason, C., & Jaffrey, S. (2012). Comprehensive Analysis of mRNA Methylation Reveals Enrichment in 3′ UTRs and near Stop Codons. *Cell, 149*(7), 1635-1646. https://doi.org/10.1016/j.cell.2012.05.003

Min, K., Zealy, R., Davila, S., Fomin, M., Cummings, J., & Makowsky, D. et al. (2018). Profiling of m6A RNA modifications identified an age-associated regulation of AGO2 mRNA stability. *Aging Cell, 17*(3), e12753. https://doi.org/10.1111/acel.12753

Müller, C., Zidek, L., Ackermann, T., de Jong, T., Liu, P., & Kliche, V. et al. (2018). Reduced expression of C/EBPβ-LIP extends health and lifespan in mice. *Elife, 7*. https://doi.org/10.7554/elife.34985

Müller, C., Zidek, L., Eichwald, S., Kortman, G., Koster, M., & Calkhoven, C. (2022). Enhanced C/EBPβ function promotes hyperplastic versus hypertrophic fat tissue growth and prevents steatosis in response to high-fat diet feeding. *Elife, 11*. https://doi.org/10.7554/elife.62625

Nerlov, C. (2010). Transcriptional and translational control of C/EBPs: The case for “deep” genetics to understand physiological function. *Bioessays, 32*(8), 680-686. https://doi.org/10.1002/bies.201000004

Niehrs, C., & Calkhoven, C. (2020). Emerging Role of C/EBPβ and Epigenetic DNA Methylation in Ageing. *Trends In Genetics, 36*(2), 71-80. https://doi.org/10.1016/j.tig.2019.11.005

Peng, S., Xiao, W., Ju, D., Sun, B., Hou, N., & Liu, Q. et al. (2019). Identification of entacapone as a chemical inhibitor of FTO mediating metabolic regulation through FOXO1. *Science Translational Medicine, 11*(488). https://doi.org/10.1126/scitranslmed.aau7116

Ramji, D., & Foka, P. (2002). CCAAT/enhancer-binding proteins: structure, function and regulation. *Biochemical Journal, 365*(3), 561-575. https://doi.org/10.1042/bj20020508

Roundtree, I., Evans, M., Pan, T., & He, C. (2017). Dynamic RNA Modifications in Gene Expression Regulation. *Cell, 169*(7), 1187-1200. https://doi.org/10.1016/j.cell.2017.05.045

Schäfer, A., Mekker, B., Mallick, M., Vastolo, V., Karaulanov, E., & Sebastian, D. et al. (2018). Impaired DNA demethylation of C/EBP sites causes premature aging. *Genes &Amp; Development, 32*(11-12), 742-762. https://doi.org/10.1101/gad.311969.118

Schöller, E., Weichmann, F., Treiber, T., Ringle, S., Treiber, N., & Flatley, A. et al. (2018). Interactions, localization, and phosphorylation of the m6A generating METTL3–METTL14–WTAP complex. *RNA, 24*(4), 499-512. https://doi.org/10.1261/rna.064063.117

Shi, H., Wei, J., & He, C. (2019). Where, When, and How: Context-Dependent Functions of RNA Methylation Writers, Readers, and Erasers. *Molecular Cell, 74*(4), 640-650. https://doi.org/10.1016/j.molcel.2019.04.025

Sterken, B., Ackermann, T., Müller, C., Zuidhof, H., Kortman, G., & Hernandez-Segura, A. et al. (2022). C/EBPβ isoform-specific regulation of migration and invasion in triple-negative breast cancer cells. *Npj Breast Cancer, 8*(1). https://doi.org/10.1038/s41523-021-00372-z

Sun, H., Li, K., Zhang, X., Liu, J., Zhang, M., Meng, H., & Yi, C. (2021). m6Am-seq reveals the dynamic m6Am methylation in the human transcriptome. *Nature Communications, 12*(1). https://doi.org/10.1038/s41467-021-25105-5

Tang, H., Weng, J., Lee, W., Hu, Y., Gu, L., & Cho, S. et al. (2021). mTORC1-chaperonin CCT signaling regulates m 6 A RNA methylation to suppress autophagy. *Proceedings Of The National Academy Of Sciences, 118*(10). https://doi.org/10.1073/pnas.2021945118

Tsukada, J., Yoshida, Y., Kominato, Y., & Auron, P. (2011). The CCAAT/enhancer (C/EBP) family of basic-leucine zipper (bZIP) transcription factors is a multifaceted highly-regulated system for gene regulation. *Cytokine, 54*(1), 6-19. https://doi.org/10.1016/j.cyto.2010.12.019

Villa, E., Sahu, U., O'Hara, B., Ali, E., Helmin, K., & Asara, J. et al. (2021). mTORC1 stimulates cell growth through SAM synthesis and m6A mRNA-dependent control of protein synthesis. *Molecular Cell, 81*(10), 2076-2093.e9. https://doi.org/10.1016/j.molcel.2021.03.009

Wang, W., Xia, X., Mao, L., & Wang, S. (2019). The CCAAT/Enhancer-Binding Protein Family: Its Roles in MDSC Expansion and Function. *Frontiers In Immunology, 10*. https://doi.org/10.3389/fimmu.2019.01804

Wang, X., Huang, N., Yang, M., Wei, D., Tai, H., & Han, X. et al. (2017). FTO is required for myogenesis by positively regulating mTOR-PGC-1α pathway-mediated mitochondria biogenesis. *Cell Death &Amp; Disease, 8*(3), e2702-e2702. https://doi.org/10.1038/cddis.2017.122

Wethmar, K., Bégay, V., Smink, J., Zaragoza, K., Wiesenthal, V., & Dörken, B. et al. (2010). C/EBPβΔuORF mice—a genetic model for uORF-mediated translational control in mammals. *Genes &Amp; Development, 24*(1), 15-20. https://doi.org/10.1101/gad.557910

Wiener, D., & Schwartz, S. (2020). The epitranscriptome beyond m6A. *Nature Reviews Genetics, 22*(2), 119-131. https://doi.org/10.1038/s41576-020-00295-8

Wu, Z., Shi, Y., Lu, M., Song, M., Yu, Z., & Wang, J. et al. (2020). METTL3 counteracts premature aging via m6A-dependent stabilization of MIS12 mRNA. *Nucleic Acids Research, 48*(19), 11083-11096. https://doi.org/10.1093/nar/gkaa816

Yang, S., Wei, J., Cui, Y., Park, G., Shah, P., & Deng, Y. et al. (2019). m6A mRNA demethylase FTO regulates melanoma tumorigenicity and response to anti-PD-1 blockade. *Nature Communications, 10*(1). https://doi.org/10.1038/s41467-019-10669-0

Zaccara, S., Ries, R., & Jaffrey, S. (2019). Reading, writing and erasing mRNA methylation. *Nature Reviews Molecular Cell Biology, 20*(10), 608-624. https://doi.org/10.1038/s41580-019-0168-5

Zhang, X., Wang, F., Wang, Z., Yang, X., Yu, H., & Si, S. et al. (2020). ALKBH5 promotes the proliferation of renal cell carcinoma by regulating AURKB expression in an m6A-dependent manner. *Annals Of Translational Medicine, 8*(10), 646-646. https://doi.org/10.21037/atm-20-3079

Zhou, J., Wan, J., Shu, X., Mao, Y., Liu, X., & Yuan, X. et al. (2018). N6-Methyladenosine Guides mRNA Alternative Translation during Integrated Stress Response. *Molecular Cell, 69*(4), 636-647.e7. https://doi.org/10.1016/j.molcel.2018.01.019

Zhu, S., Wang, J., Chen, D., He, Y., Meng, N., & Chen, M. et al. (2020). An oncopeptide regulates m6A recognition by the m6A reader IGF2BP1 and tumorigenesis. *Nature Communications, 11*(1). https://doi.org/10.1038/s41467-020-15403-9

Zidek, L., Ackermann, T., Hartleben, G., Eichwald, S., Kortman, G., & Kiehntopf, M. et al. (2015). Deficiency inmTORC1-controlledC/EBPβ-mRNAtranslation improves metabolic health in mice. *EMBO Reports, 16*(8), 1022-1036. https://doi.org/10.15252/embr.201439837

Zuidhof, H. (2022-B). Translational control of C/EBPβ isoform expression. A focus on regulation and function in breast cancer. *PhD Thesis.* University of Groningen. https://doi.org/10.33612/diss.222293305

Zuidhof, H., & Calkhoven, C. (2022-A). Oncogenic and Tumor-Suppressive Functions of the RNA Demethylase FTO. *Cancer Research, 82*(12), 2201-2212. https://doi.org/10.1158/0008-5472.can-21-3710

Supplementary figures

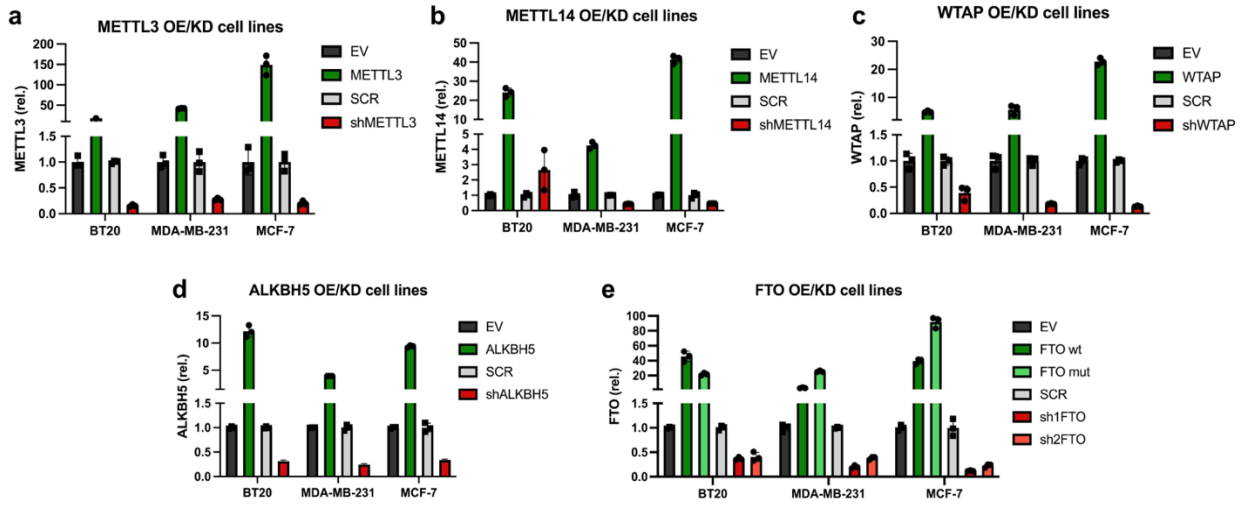

Supplementary Figure 1. RT-qPCR confirmation of selected genes overexpressed or knocked-down in BT20, MDA-MB-231 and MCF-7 cell lines. a| *METTL3* transcript quantification confirmation of OE and KD. **b**| *METTL14* transcript quantification for confirmation of OE and KD. **c**| *WTAP* transcript quantification for confirmation of OE and KD. METTL14 KD in BT20 presented an unexpected increase in its RNA levels. **d**| *ALKBH5* transcript quantification for confirmation of OE and KD. **e**| *FTO* transcript quantification for confirmation of OE (*FTO* wt/mut) and KD (sh1*FTO* and sh2*FTO*). Actin was used as RNA level normalization control for all genes shown.

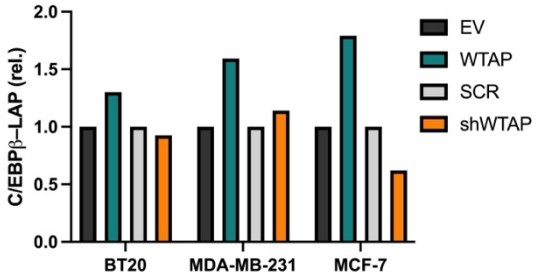

Supplementary Figure 2. C/EBPβ–LAP fraction quantification of immunoblot (Fig. 5). A marked increase in the LAP fraction is seen upon WTAP OE, whereas a slight decrease is seen in the KD cell lines. Total C/EBPβ–LAP was normalized to β-actin.

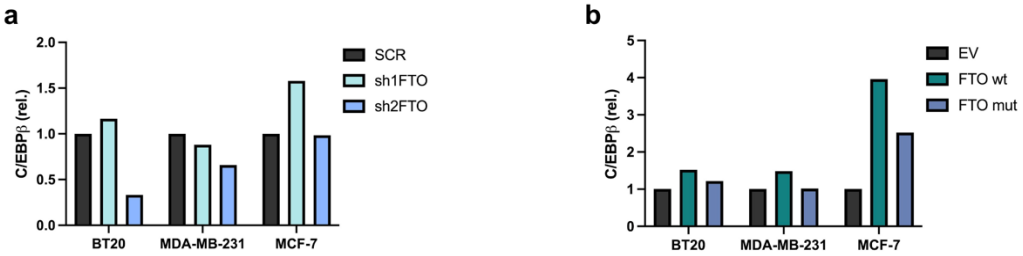

Supplementary Figure 3. C/EBPβ protein quantification in BT20, MDA-MB-231 and MCF-7 cell lines. a| FTO KD, performed with sh1FTO and sh2FTO, yielded different results in the total C/EBPβ content despite them having the same target. **b**| FTO OE of the wild-type FTO (FTO wt) and the R316.322Q mutant (FTO mut). FTO wt increased C/EBPβ levels substantially, whereas this increase was milder in the mutant counterpart. Total C/EBPβ was normalized to β-actin.

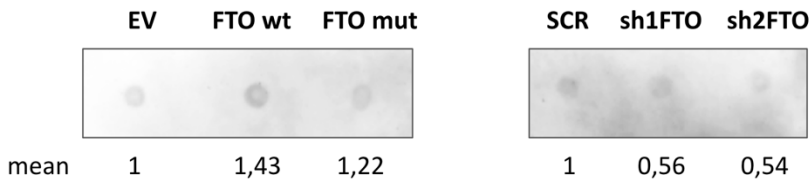

Supplementary Figure 4. N^6-methyladenosine (m^{6}A) dot blot of 26.5ng/µL (2µL/drop) of the BT20-infected cell line. Either OE of FTO wt/mut or KD with sh1FTO or sh2FTO was done in BT20s. Results show an unclear increase in methylation in FTO-overexpressed BT20s, while the opposite is seen for the FTO-knocked-down cell line. Due to low sample loading and/or irregular background noise, quantification of these results should not be exempt of technical reassessment. The mean represents the average of two independent measurements.

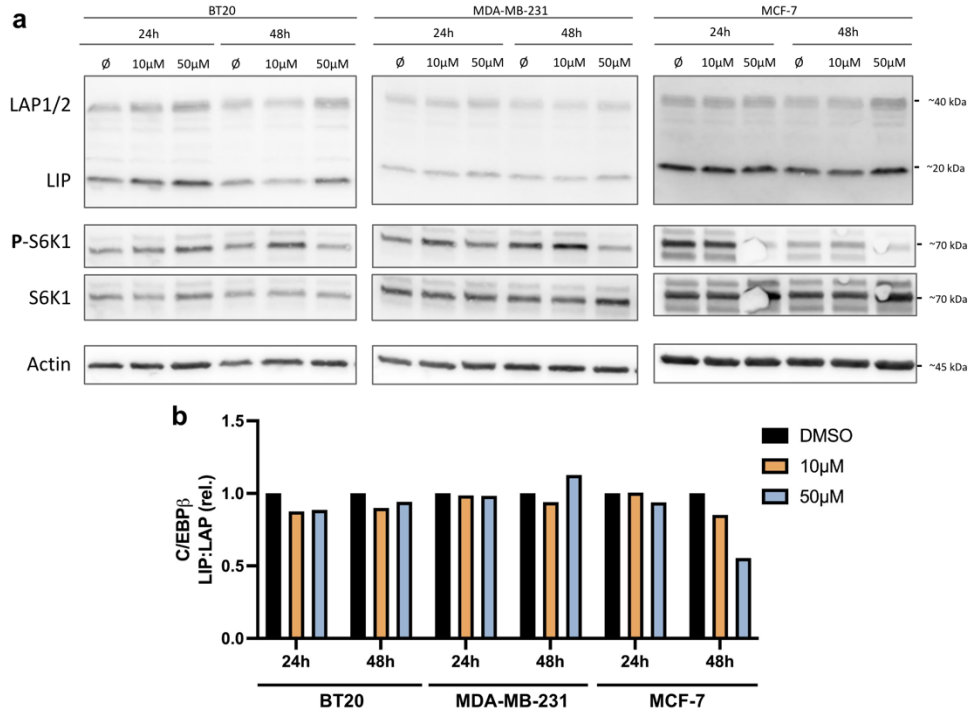

Supplementary Figure 5. C/EBPβ–LIP:LAP ratio of entacapone-treated (10µM or 50µM) cell lines (BT20, MDA-MB-231 and MCF-7) after 24h and 48h. a| Immunoblot of the described conditions. **b**| Immunoblot quantification. Entacapone showed little to no effect prior to 72h-treatment, except in the MCF-7 cell line, which appeared to be the most sensitive one. Remarkably, no increase is seen in the LIP:LAP ratio except for MDA-MB-231s after 48h at 50µM entacapone.

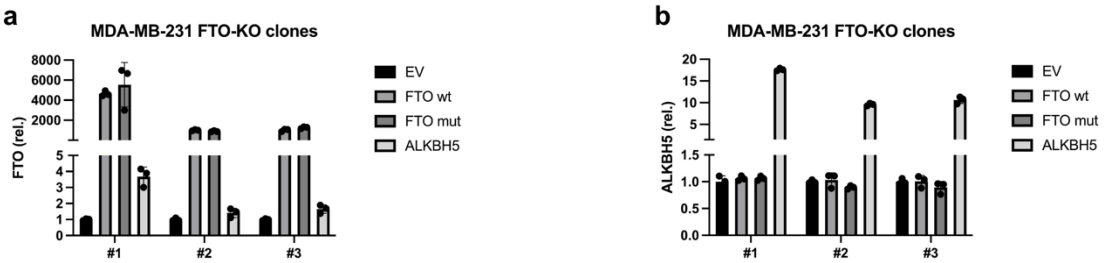

Supplementary Figure 4. RT-qPCR confirmation of selected genes overexpressed in MDA-MB-231 FTO KO clones. a| *FTO* (wt/mut) transcript quantification confirmation of the overexpression event. Remarkably high relative values indicate that non-overexpressed clones harbor no *FTO* transcripts, since they are devoid of them (tendency to infinite). **b**| *ALKBH5* transcript quantification confirmation of its overexpression.

Supplementary tables

Antibody	Ab. number	Raised in	Dilution	Diluted in	Supplier	Catalog number
C/EBPβ	14	Rabbit	1:1000	5% milk (TBST)	abcam®	ab32358
p70 S6 kinase 1	37	Rabbit	1:1000	5% milk (TBST)	Cell Signaling Technology®	CST 9202
β-Actin	88	Mouse	1:13.333	5% milk (TBST)	Proteintech®	20536-1-AP
FTO	83	Rabbit	1:1667	5% milk (TBST)	Novus Biologicals®	NB110-60935
METTL3	120	Rabbit	1:1000	5% BSA (TBST)	Cell Signaling Technology®	CST 96391
METTL14	121	Rabbit	1:1000	5% BSA (TBST)	Cell Signaling Technology®	CST 51104
WTAP	122	Rabbit	1:1000	5% milk (TBST)	Cell Signaling Technology®	CST 56501
ALKBH5	123	Rabbit	1:500	5% milk (TBST)	ThermoFisher Scientific®	PA5-67839
N^6-methyl-adenosine	125	Rabbit	1:1000	5% BSA (TBST)	abcam®	ab151230
phospho–S6 kinase 1	21 (box 3)	Rabbit	1:1000	5% milk (TBST)	Cell Signaling Technology®	CST 9206

Supplementary Table 1. Primary antibody list used for either Western Blot or methylation dot blot assay. phoshpho-S6 kinase 1 antibody is found in phospho-antibody box #3, which has its own numbering. The rest of the primary antibodies follow the general numbering for boxes #1, #2 and #4.

Oligo name	Oligo number	Supplier	5’-3’ sequence
hActin_q_Fw_1	72	Sigma-Aldrich®	CCAACCGCGAGAAGATGA
hActin_q_Rv_1	73	Sigma-Aldrich®	CCAGAGGCGTACAGGGATAG
hGAPDH_q_Fw_1	82	Sigma-Aldrich®	TCAACGGATTTGGTCGTATTG
hGAPDH_q_Rv_1	83	Sigma-Aldrich®	TCTCGCTCCTGGAAGATGG
hCEBPb_q_Fw_1	74	Sigma-Aldrich®	TTTCGAAGTTGATGCAATCG
hCEBPb_q_Rv_1	75	Sigma-Aldrich®	CAACAAGCCCGTAGGAACAT
hMETTL3_q_Fw_1	48	Sigma-Aldrich®	CAAGCTGCACTTCAGACGAA
hMETTL3_q_Rv_1	49	Sigma-Aldrich®	CAAGCTGCACTTCAGACGAA
hMETTL14_q_Fw_1	50	Sigma-Aldrich®	GTTGGAACATGGATAGCCGC
hMETTL14_q_Rv_1	51	Sigma-Aldrich®	CAATGCTGTCGGCACTTTCA
hWTAP_q_Fw_1	52	Sigma-Aldrich®	TTCCCAAGAAGGTTCGATTG
hWTAP_q_Rv_1	53	Sigma-Aldrich®	TGCAGACTCCTGCTGTTGTT
hALKBH5_q_Fw_1	62	Sigma-Aldrich®	CGGCGAAGGCTACACTTACG
hALKBH5_q_Rv_1	63	Sigma-Aldrich®	CGGCGAAGGCTACACTTACG
hFTO_q_Fw_2	17	Sigma-Aldrich®	GGAGGGTGTGACAAATGCTGTG
hFTO_q_Rv_2	18	Sigma-Aldrich®	GCAGAGGCATCGAAGCATCATC

Supplementary Table 2. Primer list (forward and reverse) for RT-qPCR.

Oligo name	Supplier	5’-3’ sequence
hMETTL3 For	Sigma-Aldrich®	GCGAAGCTTATTCGAGAGGTGTCAGGG
hMETTL3 Rev	Sigma-Aldrich®	GCGTCTAGATTCTTAGCTCTGTAAGGAAG
hMETTL3 EcoRev	Sigma-Aldrich®	CATAGTCACAGAATTCTTGCAC
hMETTL3 EcoFor	Sigma-Aldrich®	CCAAGTGCAAGAATTCTGTGAC
hWTAP For	Sigma-Aldrich®	GCACGAATTCACCTTTCCTCTCCTGGCG
hWTAP Rev	Sigma-Aldrich®	GCCTCTAGACACTGTATAAAAATTTGCTG
hWTAP AatRev	Sigma-Aldrich®	GAAATCCAGACCCAGACGTCC
hWTAP AatFor	Sigma-Aldrich®	GTAATGGTAGCTCCTCCCGCC
hALKBH5 For	Sigma-Aldrich®	GAGCGAATTCGGAGGACCCTAGAGCAGCGTC
hALKBH5 Rev	Sigma-Aldrich®	CTGTCTAGACTCAGTGCCGCCGCATC

Supplementary Table 3. Custom primer list (forward and reverse) used for the cloning of METTL3, WTAP and ALKBH5. METTL3 and WTAP were cloned in a two-fragment fashion, later on ligated through an internal EcoRI site (METTL3) or AatII site (WTAP).

Acknowledgments

The present work could not have been possible without the attention, input and commitment of Christine, who supervised my work throughout the length of my first M.Sc. internship. Christine was essential in the growth of my interest towards mRNA regulation in the context of epitranscriptomic modifications, which I am sure will prevail for a long time (RNA is everywhere after all!).

I also have to thank Josi for all her time spent helping me whenever I had any question. Josi always goes deep into the topic and makes sure that she fully understands what you need so she can provide the best answer. The conversations we have had will always be rewarding to me, as I found a great friend in my own laboratory group.

In times of stress, Gertrud stepped in to make sure I realized I could handle anything. Thank you very much for your tension-breaking personality: all laboratories would die to have you. I can only hope to find someone so fun and chill like you in future labs.

To Cor, thanks for the support and help you offered: from your decision to take me into the group to your confidence in my research quality at the times of my promotion. I could not have done it without your implication.